

AD-A045 245

IOWA INST OF HYDRAULIC RESEARCH IOWA CITY  
FLOW-VISUALIZATION OF THREE-DIMENSIONAL BOUNDARY-LAYER SEPARATI--ETC(U)  
JUN 77 T HAN; V C PATEL  
IIHR-205

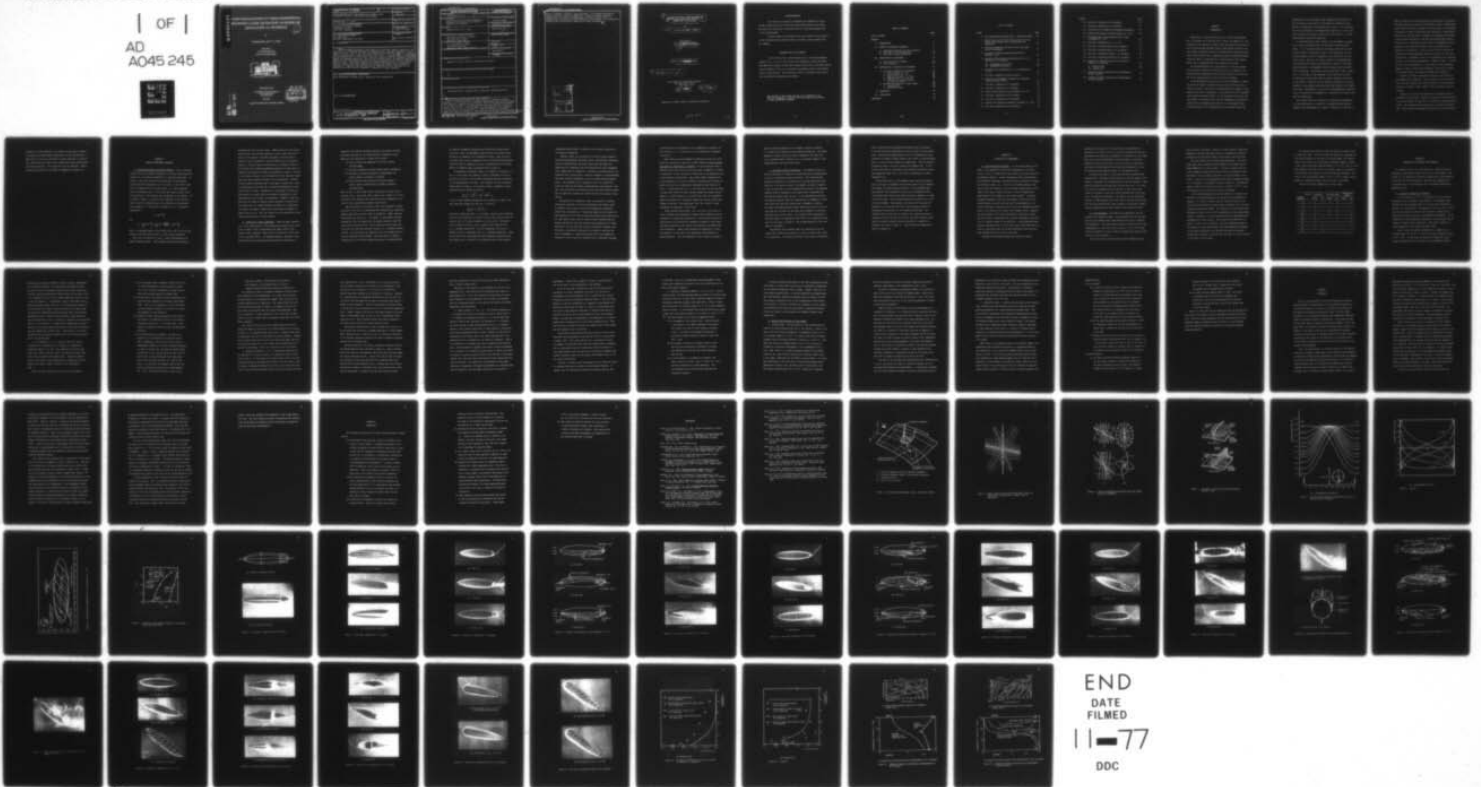
F/G 20/4

DAA629-76-G-0036

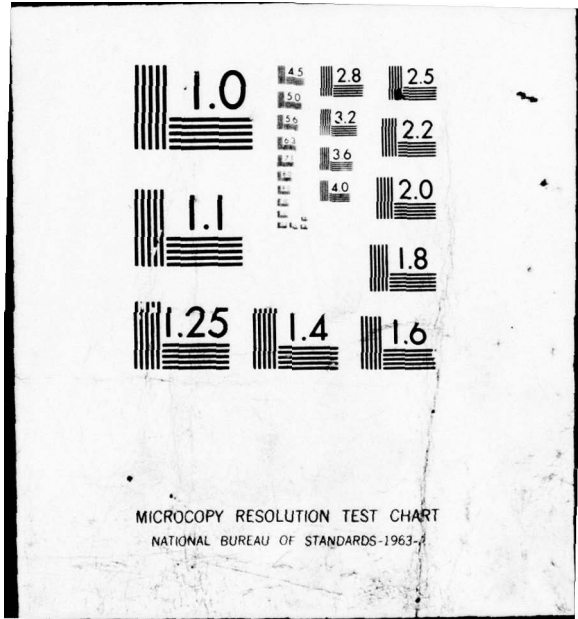
NL

UNCLASSIFIED

| OF |  
AD  
A045 245



END  
DATE  
FILMED  
11-77  
DDC



MICROCOPY RESOLUTION TEST CHART  
NATIONAL BUREAU OF STANDARDS-1963-A

AD A 045 245

# FLOW-VISUALIZATION OF THREE-DIMENSIONAL BOUNDARY-LAYER SEPARATION ON BODIES OF REVOLUTION AT INCIDENCE

me

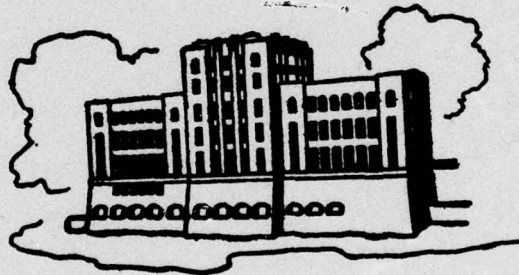
by

Taeyoung Han and V. C. Patel

Sponsored by

U.S. Army Research Office

Grant No. DAAG29-78-G-0036

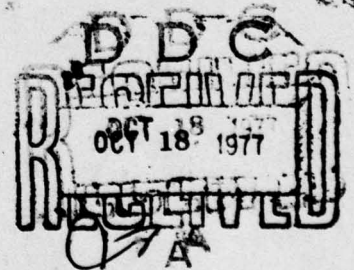


IIHR Report No. 205

Iowa Institute of Hydraulic Research  
The University of Iowa  
Iowa City, Iowa

June 1977

Approved for public release; distribution unlimited



AD No. \_\_\_\_\_  
DDC FILE COPY

<b>BIBLIOGRAPHIC DATA SHEET</b>		<b>1. Report No.</b> TIHR-205	<b>2.</b>	<b>3. Recipient's Accession No.</b>	
<b>4.</b> Flow-Visualization of Three-Dimensional Boundary-Layer Separation on Bodies of Revolution at Incidence				<b>5. Report Date</b> June 1977	
				<b>6.</b>	
<b>7.</b> Taeyoung Han, V.C. Patel				<b>8. Performing Organization Report No.</b>	
<b>9. Performing Organization Name and Address</b> Institute of Hydraulic Research University of Iowa Iowa City, Iowa 52242				<b>10. Project Task Work Unit No.</b>	
				<b>11. Contract Grant No.</b> DAAG29-76-G-0036	
<b>12. Sponsoring Organization Name and Address</b> U.S. Army Research Office P.O. Box 12211 Research Triangle Park, NC 27709				<b>13. Type of Report &amp; Period Covered</b>	
				<b>14.</b>	
<b>15. Supplementary Notes</b>					
<b>16. Abstracts</b> Surface streamline patterns on three bodies of revolution, namely a spheroid, a low-drag body and a hemisphere-hemispheroid combination body, have been examined at several angles of attack. Most of the tests were performed at low Reynolds numbers in a hydraulic flume using colored dye to make the surface flow visible. A limited number of experiments was also carried out in a wind tunnel, using wool tufts, to study the influence of Reynolds number and turbulent separation. The study has verified some of the important qualitative features of three-dimensional separation criteria proposed earlier by Maskell, Lighthill, Wang and others. The observed locations of laminar separation lines on a spheroid at various incidences have been compared with the numerical boundary-layer solutions of Wang, and it is suggested that the quantitative differences may be attributed to the significant viscous-inviscid interaction, especially at large incidences.					
<b>17. Key Words and Document Analysis. 17a. Descriptors</b> Three-dimensional, boundary-layer, separation, flow-visualization					
<b>17b. Identifiers Open-Ended Terms</b>					
<b>17c. COSATI Field/Group</b>					
<b>18. Availability Statement</b> No restriction on distribution. Available from National Technical Information Service, Springfield, VA 22161				<b>19. Security Class. This Report</b> UNCLASSIFIED	
				<b>20. Security Class. This Page</b> UNCLASSIFIED	
				<b>21. Number of Pages</b> 69	
				<b>22. Price</b>	

REPORT DOCUMENTATION PAGE		READ INSTRUCTIONS BEFORE COMPLETING FORM
1. REPORT NUMBER IIHR Report No 205	2. GOVT ACCESSION NO.	3. RECIPIENT'S CATALOG NUMBER
4. TITLE (and Subtitle) Flow-Visualization of Three-Dimensional Boundary-Layer Separation on Bodies of Revolution at Incidence	5. TYPE OF REPORT & PERIOD COVERED Technical Report	
	6. PERFORMING ORG. REPORT NUMBER IIHR Report No. 205	
7. AUTHOR(s) Taeyoung Han and V.C. Patel	8. CONTRACT OR GRANT NUMBER(s) DAAG29-76-G-0036 <i>new</i>	
9. PERFORMING ORGANIZATION NAME AND ADDRESS Institute of Hydraulic Research The University of Iowa Iowa City, Iowa 52240	10. PROGRAM ELEMENT, PROJECT, TASK AREA & WORK UNIT NUMBERS	
11. CONTROLLING OFFICE NAME AND ADDRESS U.S. Army Research Office Post Office Box 12211 Research Triangle Park, NC 27709	12. REPORT DATE June 1977	
	13. NUMBER OF PAGES 69	
14. MONITORING AGENCY NAME & ADDRESS (if different from Controlling Office)	15. SECURITY CLASS. (of this report) Unclassified	
	15a. DECLASSIFICATION/DOWNGRADING SCHEDULE NA	
16. DISTRIBUTION STATEMENT (of this Report)  Approved for public release, distribution unlimited		
17. DISTRIBUTION STATEMENT (of the abstract entered in Block 20, if different from Report)  NA		
18. SUPPLEMENTARY NOTES		
19. KEY WORDS (Continue on reverse side if necessary and identify by block number)  Three-dimensional, boundary-layer, separation, flow-visualization		
20. ABSTRACT (Continue on reverse side if necessary and identify by block number) Surface streamline patterns on three bodies of revolution, namely a spheroid, a low-drag body and a hemisphere-hemispheroid combination body, have been examined at several angles of attack. Most of the tests were performed at low Reynolds numbers in a hydraulic flume using colored dye to make the surface flow visible. A limited number of experiments was also carried out in a wind tunnel, using wool tufts, to study the influence of Reynolds number and turbulent separation. The study has verified some of the important qualitative features of three-dimensional separation criteria proposed (cont)		

18

*Next Page*

Unclassified

SECURITY CLASSIFICATION OF THIS PAGE(When Data Entered)

earlier by Maskell, Lighthill, Wang and others. The observed locations of laminar separation lines on a spheroid at various incidences have been compared with the numerical boundary-layer solutions of Wang, and it is suggested that the quantitative differences may be attributed to the significant viscous-inviscid interaction, especially at large incidences.

ADDITIONAL INFO		
NTIS	Work Section	<input checked="" type="checkbox"/>
DDC	Ref Section	<input type="checkbox"/>
UNANNOUNCED		<input type="checkbox"/>
CLASSIFICATION		
DISTRIBUTION/AVAILABILITY CODES		
RIEL	AVAIL. DFC/M	SPECIAL
A		

Unclassified

SECURITY CLASSIFICATION OF THIS PAGE(When Data Entered)

6 FLOW-VISUALIZATION OF THREE-DIMENSIONAL  
BOUNDARY-LAYER SEPARATION ON BODIES OF  
REVOLUTION AT INCIDENCE

10 by  
Taeyoung Han and V.C. Patel

Sponsored by  
U.S. Army Research Office  
Grant No. DAAG29-76-G-0036

15

14 IIHR [redacted] - 265

9 Technical rept.,

Iowa Institute of Hydraulic Research  
The University of Iowa  
Iowa City, Iowa

11 Jun 1977

12 78 p.

Approved for public release; distribution unlimited

188300

at

#### ACKNOWLEDGEMENTS

The authors are grateful to Professor B.R. Ramaprian for many helpful suggestions and criticisms during the final stages of this study. The support provided by Mr. Dale Harris and the Institute workshop staff is also acknowledged.

Partial support was provided in the final stages of this research by the Lockheed-Georgia Company, Marietta, Georgia, under Purchase Order No. CN68862.

#### IMPORTANT NOTE TO THE READER

Due to difficulties in mass-reproduction of colored photographs, Figures 9, 12, 15, 17, 22, and 23 have been reproduced in black and white. The demarcation between the blue dye injected at the front of the body and the red dye injected at the tail is therefore indicated by means of bold dotted lines in these figures. The references to dyes of different colors made in the text should be interpreted accordingly.

THE FINDINGS IN THIS REPORT ARE NOT TO BE CONSTRUED AS AN  
OFFICIAL DEPARTMENT OF THE ARMY POSITION, UNLESS SO DESIGNATED  
BY OTHER AUTHORIZED DOCUMENTS



## TABLE OF CONTENTS

	Page
LIST OF FIGURES	iv
CHAPTER	
I. INTRODUCTION	1
II. REVIEW OF PERTINENT LITERATURE	5
A. Limiting Streamlines and their Topology	5
B. Separation in Three Dimensions	6
C. Flow Past a Body of Revolution	11
III. DESCRIPTION OF EXPERIMENTS	13
A. Test Facilities and Models	13
B. Test Procedures	14
IV. OBSERVATIONS OF DETAILED FLOW PATTERNS	17
A. Flow Past a Spheroid at Incidence	17
1. Zero Incidence ( $\alpha = 0^\circ$ )	17
2. Low Incidence ( $\alpha = 5^\circ$ )	18
3. Moderate Incidence ( $\alpha = 10^\circ$ )	20
4. High Incidence ( $\alpha = 20^\circ, 30^\circ$ )	22
5. Influence of Reynolds Number ( $\alpha = 0^\circ, 20^\circ, 40^\circ$ )	24
B. Surface Flow Patterns on Other Shapes	25
1. Low-Drag Body	25
2. Combination Body	27
V. DISCUSSION	30
VI. CONCLUSIONS	35
REFERENCES	38

## LIST OF FIGURES

Figure	Page
1. Three Dimensional Boundary Layer: Definition Sketch	40
2. Typical Pattern of Skin-Friction Lines (full) and Vortex Lines (broken) near a Saddle Point of Separation	41
3. Limiting Streamlines and Vortex Lines near Nodal Point of Attachment	42
4. Two Models of Three-Dimensional Separations (Maskell, 1955)	43
5. Potential-Flow Pressure Distribution Over a 4.3:1 Spheroid at 30° Incidence	44
(a) Circumferential Direction	44
(b) Longitudinal Direction	45
6. Potential-Flow Streamlines on a 4.3:1 Spheroid at $\alpha = 30^\circ$	46
7. Flow Past a Spheroid at Zero Incidence	47
8. Locations of Axisymmetric Separation on Spheroid (Chang and Patel, 1975)	48
9. Flow Past a Spheroid at 5° Incidence	49
10. Flow Past a Spheroid at 5° Incidence	50
11. Surface Flow Patterns at Low Incidence ( $\alpha = 5^\circ$ )	51
12. Flow Past a Spheroid at 10° Incidence	52
13. Flow Past a Spheroid at 10° Incidence	53
14. Surface Flow Patterns at Moderate Incidence ( $\alpha = 10^\circ$ )	54
15. Flow Past a Spheroid at 20° Incidence	55

Figure	Page
16. Flow Past a Spheroid at 20° Incidence	56
17. Flow Past a Spheroid at 30° Incidence	57
18. Illustrations of Primary and Secondary Separations	58
19. Surface Flow Patterns at High Incidence ( $\alpha = 30^\circ$ )	59
20. Flow Entrainment on the Leeward Side of Plane of Symmetry ( $\alpha \sim 40^\circ$ )	60
21. Flow Past a Spheroid at $R_e = 7 \times 10^5$	61
22. Flow Past a Low-Drag Body at Zero Incidence	62
23. Flow Past a Low-Drag Body at 20° Incidence	63
24. Flow Past a Combination Body at 10° Incidence	64
25. Flow Past a Combination Body at 40° Incidence	65
26. Locations of Separation Point on the Plane of Symmetry of a Spheroid	66
(a) Windward Side	66
(b) Leeward Side	67
27. Comparison between Calculations and Experiments at Low Incidence	68
28. Comparison between Calculations and Experiments at High Incidence	69

## CHAPTER I

## INTRODUCTION

Separation is a generic name given to a class of flow phenomena. As pointed out by Nash and Patel (1972), for example, one, and perhaps the most important, feature which characterizes this class is that the flow becomes detached from the body surface allowing a viscous region of indefinite extent to develop between the body and the outer, quasi-inviscid flow. Separation provides a mechanism whereby vorticity, which in attached flow is confined within the boundary layer, can be transported into the interior of the fluid.

In three-dimensional flow, the definition of the term "separation" has been a subject of controversy since it is generally observed that flow detachment from the surface cannot be related simply to the characteristics of the flow near the surface.

In two-dimensional flow, the point of flow detachment or separation from the surface coincides with the point at which the skin friction vanishes. This point is characterized by a number of other features which occur concurrently. Among these are (a) the boundary-layer equations become singular, (b) the direction of the flow near the surface is reversed so that the flow downstream of separation is inaccessible to boundary-layer analysis, (c) the boundary layer thickens rapidly in the neighborhood of the separation point and

consequently the usual boundary-layer assumptions break down, and (d) the pressure distribution at and beyond the separation point ceases to conform with the potential-flow solution. The coincidence of all these phenomena in two-dimensional steady flow is well recognized although the condition of zero wall shear stress is the most often quoted criterion for separation.

In three-dimensional flows, however, flow detachment or separation is rarely associated with the vanishing of the wall shear stress. It is recognized that the wall shear stress does not fall to zero except in a few special cases. More frequently, the skin friction remains finite at a separation line and may even be relatively large. There are, of course, regions in three-dimensional flows which may be treated by extending the concepts of two-dimensional separation via detachment from the surface and inaccessibility from upstream. As pointed out by Nash and Patel (1972), separation - in the sense of the detachment of the flow from the body - is sometimes not associated with any special character of the flow at the surface. These can best be studied by examining the overall features of the boundary-layer flow rather than those of the surface flow alone. Nevertheless, discussion of three-dimensional separation in the literature has concentrated on its definition in terms of surface flow conditions.

The present study was conceived as a preliminary investigation to a more ambitious one in which it is proposed to make detailed boundary-layer measurements on a body of revolution at incidence in

order to obtain a more precise quantitative definition of separation. The main objective of this work is therefore to make a comprehensive visual study of the basic features of the flow past a few representative shapes in order to learn more about separation in three-dimensions and, at the same time, to identify the phenomena which should be given special attention in the detailed boundary-layer explorations later on. Although the latter series of experiments will be performed at high Reynolds numbers, where the boundary layer is expected to be turbulent, it was felt that the basic features associated with three-dimensional separation would be the same with laminar flow. Consequently, most of the experiments were conducted in water, with the models suspended in a hydraulic flume. A series of tests was then undertaken in a wind tunnel at higher Reynolds numbers in order to obtain some information concerning the difference between laminar and turbulent boundary layer behaviors.

Chapter II reviews the pertinent literature associated with three-dimensional separation. Basic concepts of limiting streamlines and their topology are briefly explained and the separation criteria of Lighthill (1963), Maskell (1955), and Wang (1972) are reviewed.

Chapter III describes the experimental arrangement and test procedures that were used. Chapter IV contains a detailed description of the surface flow patterns on a spheroid at various angles of attack. The observations are discussed in the light of previous work. Some additional experiments performed on two other bodies of

revolution are also described. An attempt is then made in Chapter V to correlate the experimental observations with the calculations of Wang (1972) as far as the flow past a prolate spheroid is concerned. It is found that the results of the computations differ substantially from the observations. The reasons for this are explored. Finally, the major conclusions of the study are summarized in Chapter VI.

## CHAPTER II

## REVIEW OF PERTINENT LITERATURE

A. Limiting Streamlines and their Topology. Lines on the body surface which are everywhere tangential to the wall shear stress are referred to as "limiting streamlines" or "skin-friction lines". In general, these lines intersect the projections of the external irrotational-flow streamlines onto the surface at some finite angle which is termed the wall cross-flow angle,  $\beta_\omega$ . The streamlines within the boundary layer, on the other hand, make an angle  $\beta$  with the projections of the external flow streamlines on the surface. If, as shown in Figure 1,  $U$  and  $W$  are the components of the velocity vector within the boundary layer in the direction of the external flow streamline ( $x$  - direction) and normal to it ( $z$  - direction), respectively,

$$\beta = \tan^{-1} \frac{W}{U}$$

and

$$\beta_\omega = \lim_{y \rightarrow 0} \tan^{-1} \frac{W}{U} = \lim_{y \rightarrow 0} \tan^{-1} \frac{\partial W / \partial y}{\partial U / \partial y} = \tan^{-1} \frac{\tau_z}{\tau_x}$$

Here,  $y$  is measured normal to the surface and  $\tau_x$  and  $\tau_z$  are the components of the wall shear stress  $\tau_\omega$  in the  $x$  and  $z$  directions.

The points at which both  $\tau_x$  and  $\tau_z$  vanish simultaneously are termed "singular points". Such singular points are classified by



mathematicians into two main types: saddle points and nodal points. These features are observed typically at points where the flow attaches to the surface or detaches (separates) from the surface. Lighthill (1963) illustrated a typical saddle point of separation (Figure 2) and four types of nodal points of attachment (Figure 3). The possible local limiting-streamline patterns at a nodal point of separation are exactly the same as those shown in Figure 3, but with all the arrows reversed. Such singularities of the limiting streamlines have been observed in surface flow visualizations. However, the most commonly observed form is that shown in Figure 3(b), which is associated with the flow near a general three-dimensional stagnation point on a body. Recognition of the existence of such singular points in a given flow is an essential prerequisite to the understanding of the overall flow phenomena. Lighthill (1963) has shown that the range of possible overall patterns of skin-friction and vortex lines on a smooth surface are subject to a topological law, namely the number of nodal points must exceed the number of saddle points by two. This law is used in the interpretation of the observed flow patterns in later chapters.

B. Separation in Three Dimensions. Among the major contributors to the understanding of three-dimensional boundary-layer separation are Moore (1956), Eichelbrenner and Oudart (1954, 1973), Maskell (1955), Lighthill (1963), Brown and Stewartson (1969), Wang (1972), and Smith (1975). As indicated earlier, a majority of the previous work has centered around correlating the occurrence of

separation with surface streamline patterns, and several criteria have been suggested for the identification of separation lines.

Among the early definitions of these may be found:

- (1) Lines on which some component of the skin friction vanishes (Wang),
- (2) Limiting streamlines joining singular points (Lighthill),
- (3) Envelope of limiting streamlines (Eichelbrenner and Oudart, Maskell, Stewartson, and Wang),
- (4) Lines dividing flow which has come from different regions (Moore, Eichelbrenner and Oudart, Lighthill, and Stewartson).

Each of these is valid under certain conditions, but none is universally valid. More recent work of Wang (1972), Peake et al (1972), and Smith (1975) suggests that separation may be accompanied by one or more of the surface flow features listed above.

The pioneering work of Maskell (1955) still represents a major milestone in the area of three-dimensional boundary-layer separation. Maskell identified two basic types of separation: bubble type and free-vortex type (Figure 4). The former, is also termed "singular separation" since the separation line passes through or joins singular points defined earlier. Such a separation also divides the flow which has come from different regions (i.e., upstream and downstream). The flow beyond the separation line of the bubble type is then not accessible from upstream. The free-vortex or ordinary separation does not involve singular points and is recognized only

by limiting streamlines coalescing and leaving the surface along some line. Here, the detachment from the surface is usually accompanied by the formation of a longitudinal vortex. Also, the flow on either side of such a separation line is accessible from upstream. These two types of separation are well illustrated by the classical figures in Maskell's paper (reproduced here as Figure 4).

As suggested by Lighthill (1963), the "bubble (or singular)" as well as "free vortex (or ordinary)" types of separation can be explained on the basis of the volume flow between adjacent streamlines in the neighborhood of the wall. With reference to the co-ordinate system shown in Figure 1, the velocity  $Q$  along a streamline a small distance from the surface is given by

$$\frac{1}{\mu} \left[ \tau_x^2 + \tau_z^2 \right]^{\frac{1}{2}} y = \left[ U^2 + W^2 \right]^{\frac{1}{2}} = Q$$

If two of these limiting streamlines lie a distance 'h' apart, then the volume rate through the area 'hy' is given by

$$\frac{1}{2\mu} \left[ \tau_x^2 + \tau_z^2 \right]^{\frac{1}{2}} y^2 h = \epsilon$$

Since this volume flow rate,  $\epsilon$ , is constant, there are two mechanisms by which the streamlines can greatly increase their distance from the surface, that is, by which separation can take place. Detachment will be imminent if both  $\tau_x$  and  $\tau_z$  approach zero simultaneously (i.e., singular separation), or if the streamlines run close together so that 'h' approaches zero (i.e., ordinary separation). Thus we can perceive two mechanisms of three-dimensional separation near the surface; one is related to the singular points of the limiting

streamlines and the other is related to the asymptotic behavior of the limiting streamlines.

Lighthill (1963) also disputed the envelope concept proposed earlier by Eichelbrenner and Oudart (1954), and defined a separation line as a skin-friction line which issues from both sides of a saddle point of separation and after embracing the body, disappears into a nodal point of separation. According to this definition, the separation line, being itself a limiting streamline, is distinguished from other limiting streamlines in that it passes through singular points. This suggests that a separation line is a closed curve around the body and also implies inaccessibility from upstream. However, this definition is restricted to what has been termed as bubble type of separation and does not include the free vortex type of separation.

The definition of separation lines as envelopes of limiting streamlines, proposed at first by Eichelbrenner and Oudart (1954), is somewhat loose insofar as most three-dimensional separations possess this characteristic. Definitions based on the vanishing of some component of skin friction along some direction are precise only for some special cases, such as infinite swept cylinders where an obvious direction in which the skin-friction vanishes can be easily identified. For the flow past a body of revolution, however, this definition is meaningful only when the incidence is zero and the flow is axisymmetric. Nevertheless, Wang (1972) has suggested an extension of this criterion by proposing that a separation line may

be identified by the vanishing of the circumferential component of skin friction (i.e., the reversal of the circumferential component of velocity).

Wang (1972) has revived Maskell's separation criteria by introducing the concepts of "open" and "closed" separations for the flow past bodies of revolution at incidence. An open separation line is defined as that which does not cross the plane of symmetry on a body of revolution, so that the flow on either side of the separation line is fed entirely from upstream. Wang (1974) further suggested that an open separation line may be assumed to coincide with the locus of points at which the circumferential component of skin-friction is zero. A closed separation line, on the other hand, is one that forms a closed curve around the body, passing through the singular points. However, a closed separation, as defined here, does not necessarily imply the existence of a separation bubble that closes further downstream of the body. The terminology "open" and "closed" is used throughout the remainder of this thesis.

Peake, Rainbird and Atraghji (1972) and Smith (1975) have recently reviewed three-dimensional boundary-layer separation and its importance in aeronautical applications. Both indicate clearly the limitations of the surface-flow diagnostics insofar as they cannot give much indication of the overall flow patterns that emerge from such separations. Indeed, Smith proposes two approaches, "local" and "global", to the study of the complicated flow phenomena in three-dimensions. The local approach is one in which an attempt is

made to recognize separation as it happens, seeking to identify it in terms of the behavior of the limiting streamlines. The global approach is that in which the various elements of the total flow (e.g., boundary layers, vortices, etc.) are brought together in the understanding of the entire flow field.

C. Flow Past a Body of Revolution. The boundary layers on a body of revolution at incidence are characterized by circumferential as well as longitudinal pressure gradients. The potential-flow pressure distribution on the surface of a prolate spheroid of axis ratio 4.3 at an angle of attack of 30 degrees is shown in Figure 5. It will be seen that, in the circumferential direction, the pressure gradient from the windward to the leeward side is favorable near the nose and adverse near the tail. In the longitudinal direction, the pressure gradient along the windward plane of symmetry is favorable while that along the leeward plane of symmetry is adverse. The locus of minimum pressure points, which occurs close to the leeward side over the front of the body, moves gradually to the windward side over the tail region. The potential-flow streamlines on the body surface, as computed by Choi (1977), for a spheroid of axis ratio 4.3 are shown in Figure 6. The minimum-pressure line is also shown in the figure.

The boundary layer develops under the influence of this potential-flow pressure distribution, at least in regions where there is no separation. The general direction of the limiting streamlines

can be inferred from the pressure distribution and the curvature of the potential-flow streamlines as shown in Figure 6 by the dotted lines. Beyond the minimum pressure line, the circumferential flow encounters an adverse pressure gradient and a point is reached beyond which it cannot proceed towards the leeward side. Thus the limiting streamlines begin to turn back towards the windward side. It will be seen later that at sufficiently large angles of attack the limiting streamlines merge into a line which is identified as an open separation line.

The characteristics of the boundary layer along the intersection of the plane of symmetry with the body surface on the windward and leeward side deserve special mention. On the windward side, the potential flow streamlines as well as the streamlines within the boundary layer diverge away from the plane of symmetry in either side of the plane. This line may therefore be thought of as a line of flow attachment. The boundary layer along this line would be expected to be relatively thin due to the continuous removal of low-momentum fluid from it by the streamline divergence. The boundary layer can thus grow or maintain its thickness only by entrainment of fluid from the free stream. The major features of the surface streamline patterns actually observed on a spheroid at incidence are shown in Figure 15. These features are explored in detail in Chapter IV.

CHAPTER III  
DESCRIPTION OF EXPERIMENTS

A. Test Facilities and Models. In the initial phase of the study, it was proposed to conduct the experiments in the small (36 in. x 36 in.) closed-circuit wind tunnel of the Iowa Institute of Hydraulic Research. Several techniques of flow visualization were therefore considered, including the use of machine oil, paraffin and chalk, smoke, etc. It was soon concluded, however, that none of these was suitable at the air speeds (around 60 fps) of interest, since some of these work best at very low speeds while others appear to be adequate at much higher speeds. A recently developed technique, which uses soap bubbles filled with an air-helium mixture, was also tried but had to be abandoned since it could not provide a detailed picture of the flow phenomena occurring close to the surface in the rather thin boundary layers. Emphasis was thus shifted to the well-tried method of using dye in water. The main series of experiments was therefore conducted in the 30 in. x 30 in. hydraulic flume of the Institute. A few experiments were, however, performed later on in the wind tunnel using wool tufts in order to investigate some of the gross features of flow that had been identified from the tests in the flume.

Although three different models were tested at various



incidences, the majority of the experiments were performed on a spheroid with an axis ratio of 4.3, primarily because some previous experimental and theoretical information is available for this shape. Some tests were then performed on a low-drag body of revolution proposed by Goodson and Parsons (1972) and later on a combination half-sphere and half-spheroid body which was considered as a suitable shape for more detailed studies of the boundary layer.

All models were made 16 inches long and were fabricated from seasoned wood. The models were painted and a grid was drawn on the surface to facilitate the interpretation of the flow patterns. Each model was fitted with six dye ports near the nose ( $X/L = 0.1$ , where  $X$  is the axial distance from the nose and  $L$  is the total axial length of the body) so that dye could be ejected close to the surface. The models were mounted in the flume or in the wind tunnel by means of eight support wires, four each at the nose and the tail. The wires were provided with screw couplings so that their lengths could be adjusted and the model located in the desired position.

B. Test Procedures. The models were suspended at the mid section of the hydraulic flume. Triple-strength blue and red food-coloring dyes (Neumann Buslee Wolf 646385) were used to visualize the streamlines. Since the specific gravity of this dye was in the neighborhood of 1.019, while that of water at 72°F is 0.995, some alcohol was added to the dye in order to equalize the specific gravities of the dye and water.

The dye was usually injected under gravity through the port

near the nose of the model. However, in some instances, additional features of the flow were made visible by introducing a different colored dye at appropriate places by hand using a long fine tube.

The flow features were recorded photographically. All photographs were taken through the glass sidewall of the flume using a ASAHI PENTAX-H3V (1:1.8/55) camera. In order to picture the flow on the windward, leeward and the flank side of the models at each incidence, it was therefore necessary to realign the model in the flume. A typical set of photographs taken with the spheroidal model at an incidence of 20 degrees is shown in Figure 15. The Reynolds number, based on the length of the body, is about  $8 \times 10^4$ , so that the boundary layer on the body is laminar everywhere.

In the flume experiments it was not possible to ascertain the quality of the mainstream flow with regard to the freestream turbulence. It is known, however, that the turbulence level is not low by usual wind-tunnel and water-tunnel standards, nor is the flow accurately uniform and steady. The influence of these factors must therefore be borne in mind in the interpretation of the experimental results. Secondly, it is also recognized that the experiments were performed with a free surface. These effects are expected to be small, at least at low incidences, since the submergence depth of the models was always much greater than two maximum body diameters. At the higher incidences it is possible that some free-surface effects may be present at the nose when the model is tilted vertically to obtain the side views.

The surface flow patterns in the wind tunnel were made visible by using wool tufts. It was of course not possible to reproduce the low Reynolds numbers of the flume in the wind tunnel, but observations could be made over a wide range of Reynolds numbers. Indeed, at the lowest wind-tunnel Reynolds number of  $2.5 \times 10^5$ , which is still high compared with that  $8 \times 10^4$  in the flume, some of the features of the laminar flow observed in the flume could be reproduced. The tests at the high Reynolds numbers (up to  $7 \times 10^5$ ), however, corresponded to a turbulent boundary layer over most of the model.

The following table summarizes the visual study.

Incidence (Degree)	Model		Spheroid		Low Drag Body		Combination Body	
	Water	Air	Water	Air	Water	Air	Water	Air
0°	X	X	X	X				X
2°	X							
5°	X		X	X				
10°	X		X	X				X
20°	X	X	X	X				X
30°	X							X
40°	X	X						X
50°	X							
75°			X					

## CHAPTER IV

## OBSERVATIONS OF DETAILED FLOW PATTERNS

As indicated earlier, the flow patterns on a spheroid were investigated in much greater detail than those on other shapes. The results for the spheroid are therefore presented first and discussed in the light of the previous work. These are then compared with the observations on a low-drag body and a hemisphere-hemispheroid combination body.

A. Flow Past a Spheroid at Incidence.

1. Zero Incidence ( $\alpha = 0^\circ$ ). The boundary layer on a body of revolution at zero incidence is axisymmetric. The boundary layer develops from the attachment point at the nose and if separation is present it is well defined. The separation line is a circle, concentric with the body axis, and the flow features at separation are basically the same as those at a two-dimensional separation. In the terminology of three-dimensional separation, we can classify this as singular or bubble type of separation in the sense of Maskell, or closed separation in the notation of Wang (1972).

Figure 7 shows the surface streamlines on a spheroid at a Reynolds number of  $8 \times 10^4$ . It will be seen that separation occurs at  $X/L \approx 0.80$ . In this case, the position of separation can be readily determined from the solution of the axisymmetric laminar

boundary-layer equations either by using an integral (approximate) or a differential method. The calculations performed by Chang and Patel (1975) for spheroids of various axis ratios using potential-flow pressure distributions indicate that for the present case (4.3:1 spheroid) the position of laminar separation would be at  $X/L \approx 0.85$  (see Figure 8.). Furthermore, Figure 8 also shows that the predictions made by Wang (1972) for a 4:1 spheroid (see Figure 26) are at variance with those of Chang and Patel for the same shape, the position of separation predicted by Wang (1972) being further downstream (at  $X/L \approx 0.89$ ) of that predicted by Chang and Patel. Since the separation on his 4:1 spheroid is expected to occur earlier than on a 4.3:1 spheroid, it seems that the computations of Chang and Patel (1975) agree better with results of the flow visualization than the computations of Wang (1972). Unfortunately, at non-zero incidences the calculations of Wang (1972) are the only ones available at the present time.

2. Low Incidence ( $\alpha = 5^\circ$ ). Figure 9 shows the surface streamlines on the spheroid at an incidence of 5 degrees and a Reynolds number of  $8 \times 10^4$ . Three different views are shown, namely the leeward side (top view), the flank of the body (side view) and the windward side (bottom view). Comparison between Figure 9 and Figure 7 shows immediately the complications introduced by this small incidence relative to the axisymmetric flow.

Among the major features of the flow are the following:

- (a) On the windward plane of symmetry (Figure 9(c)) there is a well defined point of flow reversal at about  $X/L = 0.84$ . The wall streamlines on either side of this plane diverge towards the leeward side.
- (b) On the flank of the body the surface streamlines converge from the windward to the leeward side (Figure 9(b)). This is to be expected in view of the potential flow behavior (Figure 6) since there is a pressure gradient in that direction.
- (c) Perhaps the most interesting feature of the flow is the change in the downward direction of the surface streamlines around  $X/L = 0.55$  (Figure 9(b)). This implies a reversal of the flow in the circumferential direction.
- (d) On the leeward plane of symmetry, the clarity of Figure 9(a) is not sufficient to identify exactly what is happening. This is partly due to the circumferential diffusion of the dye introduced upstream. In order to clarify this, the body was turned around through  $180^\circ$  so that the dye ports lay near the tail of the body, and the photographs were taken again. These views are shown in Figure 10. From the top view, it is seen that the boundary layer on the leeward side encounters reverse flow at approximately  $X/L = 0.94$ . The lateral diffusion of dye is also

seen quite clearly. The location of the point of flow reversal in the windward side is, however, somewhat different from that indicated by Figure 9(c).

The sketches in Figure 11 attempt to summarize the basic features observed from the photographs. It is seen that the points of flow reversal in the windward and leeward sides (S1 and S2) are singular saddle points of separation. The curved dotted line joining these two points shown in Figure 11(c) appears to divide the flow coming from upstream from that coming from downstream. This line is therefore a "closed separation" line in the sense of Wang (1972) or we have a bubble type of separation along this line in the sense of Maskell.

Now, since the flow from the two saddle points S1 and S2 diverges and appears to merge into the closed separation line joining S1 and S2, it is imperative that there exist a singular nodal point of separation, such as N1, toward which the flow converges. Together with a similar nodal point on the other side of the body, there are now four nodal points (A, B, N1, and N2) and two saddle points (S1 and S2) on the surface. Thus, the topological law is satisfied.

3. Moderate Incidence ( $\alpha = 10^\circ$ ). The surface streamlines on the spheroid at an angle of attack of 10 degrees are shown in Figures 12 and 13. In the former, the reversed flow near the tail has been made visible by injecting the red dye in the tail region, while in Figure 13 additional features of the flow in the tail region are shown by again turning the model around so that the surface dye ports

are located at  $X/L = 0.90$ . From Figure 12, it will be seen that at this higher incidence the divergence of the streamlines on the windside and the convergence on the leeward side are considerably greater than those observed at an incidence of 5 degrees. Secondly, it is observed that the streamline divergence on the leeward side (Figure 12(a)) over the middle of the body is now greater and leads to a merger of the streamlines. The line along which this merger occurs is identified as an open separation line (or a free-vortex separation line). Indeed, Figures 12(a) and (b) show some evidence of the tendency of the boundary layer to roll up into a longitudinal vortex along this line. This particular feature was clearly observed in the actual tests and later in a movie that was taken.

The region occupied by the red dye in Figure 12(b) and (c) is the reversed flow region and is bounded upstream by a closed (bubble type) separation line. Figure 13(a) and (c) confirm the existence of the singular separation points on the plane of symmetry along the leeward and the windward side.

The main features of the surface streamlines observed from several photographs have been sketched in Figure 14. Again two nodal points (N1, and N2 on the opposite side of the body) have been added for reasons discussed earlier. Figure 14(a) and (b) show the limiting streamlines originating from the front stagnation point and merging into the open separation line. Although very little direct experimental evidence is available either from previous work or the present photographs, it appears that the nodal points coincide



with the intersection of the lines of open and closed separations. This is shown in Figure 14(b).

The point of flow reversal on the windside (S1) occurs at approximately  $X/L = 0.89$ , while that on the leeward side (S2) occurs at approximately  $X/L = 0.98$ . The locations of these points are obviously important in the determination of the overall flow pattern and will be discussed later in the light of the results of previous experiments and calculations.

4. High Incidence ( $\alpha = 20^\circ, 30^\circ$ ). The surface streamlines at  $\alpha = 20$  degrees are shown in the Figures 15 and 16, while those at  $\alpha = 30$  degrees are presented in Figure 17. It will be seen from Figures 15 and 16 that the basic flow features at  $\alpha = 20$  degrees are quite similar to those discussed earlier for  $\alpha = 10$  degrees. However, a more careful examination of these figures in conjunction with similar photographs taken at other instances of time and the observation of the actual flow in the flume indicated that a new phenomena occurs at incidences of the order of 20 degrees. This is the existence of a secondary open type of separation and reattachment. This phenomenon is apparent from Figure 17 which corresponds to an incidence of 30 degrees and particularly in Figure 18(a) which was taken by injecting a puff of red dye near the nose of the model. Figures 17(b) and 18(a) show three different lines running down the side of the model: the lowest one corresponding to the primary open-type of separation, the upper corresponding to a secondary open-type of separation, and the middle indicating an open-type of

reattachment. Figure 18(b) attempts to convey a cross-sectional view of the flow in the neighborhood of the mid-body.

Since the open-type of separation lines are characterized by convergence of surface streamlines into them, the open-type of reattachment line located between them is identified by a strong divergence of surface streamlines emanating from it. This and other features of limiting streamlines on a spheroid at high angles of incidence are illustrated in Figure 19. Again it is postulated that the lines of open separation terminate at singular nodal points of separation N1 and N2 on the closed separation line, and correspondingly, the open-type of reattachment line terminates at a singular saddle point of separation S3 on the closed separation line. Thus, there are now six nodal points and four saddle points on the surface and the topological law is satisfied.

The possible vortex pattern associated with the lines of open separation and reattachment on the side of the body is illustrated in Figure 18(b). This would indicate that there must be strong entrainment of freestream fluid along the leeward plane of symmetry. This is confirmed by Figure 20 which shows that dye injected at a point some distance away from the body on the plane of symmetry gets rapidly entrained toward the body surface and becomes a part of the two large vortex motions.

Finally, it would be seen from Figures 15 and 17 that the region of reversed flow grows in extent as the incidence increases. It appears that the reversed flow penetrates upstream along the side

of the body. There is a corresponding upstream movement of the primary open separation and hence of the lines from which the primary vortex system emanates.

5. Influence of Reynolds Number ( $\alpha = 0^\circ, 20^\circ, 40^\circ$ ). As mentioned earlier, the same spheroid model was tested in the wind tunnel using wool tufts over a wider range of Reynolds numbers in order to investigate turbulent boundary layer separation. Figure 21 shows the flow patterns at a Reynolds number of  $7 \times 10^5$  at three different angles of attack. It was observed that these patterns do not change a great deal with Reynolds numbers in the range  $2.5 \times 10^5$  to  $7.0 \times 10^5$ . The main features of the flow are summarized below:

- (a) In axisymmetric flow (Figure 21(a)), the flow pattern is the same as in the flume experiments (see Figure 7(b)) except the point of flow reversal is delayed to  $X/L \approx 0.95$  which is considerably downstream of the point of laminar separation shown in Figure 7(b) ( $X/L \approx 0.80$ ).
- (b) At an angle of attack of 20 degrees (Figure 21(b)), the wool tufts indicated the existence of an open type separation on the side and closed separation near the tail.
- (c) As the incidence is increased to 40 degrees, the sharp turning of the wool tufts in Figure 21(c) indicates the existence of an open separation. The open separation line starts further upstream with increasing incidence.

It would be obvious from Figure 21 that flow visualization using wool tufts in a wind tunnel does not give as detailed an information on the surface streamlines as dye in water. However, from the limited results presented here, it was concluded that the Reynolds number (and therefore, whether the boundary layer is laminar or turbulent) plays a significant role in the determination of the overall flow patterns on a body of revolution at incidence, but the qualitative features of the open and closed types of separation discussed earlier are present in both laminar and turbulent boundary layer separations.

#### B. Surface Flow Patterns on Other Shapes.

1. Low-Drag Body. The flow pattern on the low-drag body was found to be quite different from that on the spheroid. Figure 22 (a) and (b) show the surface streamlines in axisymmetric flow ( $\alpha = 0^\circ$ ) at a Reynolds number of  $8 \times 10^4$ . It would be seen that the laminar boundary layer on the body separates at about  $X/L = 0.56$  (i.e., soon after the location of maximum radius at  $X/L = 0.44$ ) and this is followed by a turbulent reattachment in the neighborhood of  $X/L = 0.60$ . Thus, there is a toroidal separation bubble on the surface. Figure 22 (b), taken several minutes after injecting a puff of dye in the bubble, indicates that the bubble is quite stable. It is perhaps interesting to note here that in the detailed boundary layer explorations of Patel, Lee, and Güven (1977) on this body at the much higher Reynolds number of  $1.2 \times 10^6$ , transition to turbulent

flow also occurred as a result of laminar separation followed by turbulent reattachment in the neighborhood of  $X/L = 0.475$ .

In order to eliminate the separation bubble it was decided to wrap a trip wire at the location of maximum radius. Figure 22(c) shows the axisymmetric flow with the trip wire. Due to the turbulent flow behind the wire it is now virtually impossible to identify the surface streamlines.

Figure 23 shows the flow pattern on the low-drag body at an incidence of 20 degrees. It is observed that the flow over the front half of the body shows the same qualitative features as that on the spheroid indicating the formation of an open separation line. The flow over the rear half is not altogether clear due to the turbulent boundary layer, but we can still observe the following features (a) there is no reversal of flow along the plane of symmetry on either the top (leeward) or the bottom (windward) side of the body, (b) there is a small reverse flow region (Figure 23(c)) immediately behind the trip wire (due presumably to the large wire diameter), and (c) there exists a reversed flow region on the side of the body. Although the latter feature is similar to that observed on the spheroid at moderate to large angles of attack, the reverse flow here does not appear to extend all the way to the tail.

The tests on the low-drag body reported here were conducted with a view to evaluating this shape as a possible candidate for the more detailed boundary-layer measurements. It was quickly concluded that the closed separation bubble on the body, which exists even in

axisymmetric flow, would not enable boundary-layer measurements to be made over a large portion of the body. This body therefore was discarded from further consideration. Nevertheless, it remains a practically important configuration and the study of the bubble, its distortion with incidence and other flow features would be of considerable interest in its own right.

2. Combination Body. A careful study was made of the boundary-layer thickness and other features required for detailed velocity profile measurements in a three-dimensional boundary layer. This was achieved by performing some preliminary boundary-layer calculations in axisymmetric flow and along the plane of symmetry of several different shapes and at several angles of attack. The results indicated that a combination body, obtained by adding a hemisphere to a half spheroid of axis ratio 4.0, would be a suitable body of revolution for detailed boundary-layer measurements. A 16 inch long model of such a body was therefore constructed for flow visualization studies.

When tested in the hydraulic flume at low Reynolds numbers, the combination body indicated the presence of a separation bubble on the leeward side, at the location of maximum radius, even at small angles of attack. Since the calculations mentioned earlier (which were performed for large Reynolds numbers) did not indicate such a separation, it was decided to continue the visual study on the combination body in the wind tunnel so that the influence of Reynolds number could be examined. The main results of these experiments are

summarized below:

At low incidence:

- (a) At angles of attack of about 10 degrees, and Reynolds numbers less than about  $2.4 \times 10^5$ , the wool tufts attached to the body indicated the existence of an open type of separation line on the side and a closed separation bubble on the leeward side in the neighborhood of the location of maximum radius (Figure 24(a)). The former feature is in agreement with the results of the tests on the spheroid while the latter confirmed the flume observations on the combination body.
- (b) As the Reynolds number was increased (to about  $7 \times 10^5$ ) the separation bubble near the nose disappeared (see Figure 24(b)) leaving only the open type of separation on the side.
- (c) Figures 24(a) and (b) also show that over the range of Reynolds numbers investigated there does not appear to be a closed type of separation near the tail of the body. At these Reynolds numbers the boundary layer is expected to be turbulent for some distance ahead of the separation.

At high incidence:

- (a) At angles of attack of about 40 degrees (Figure 25), the wool tufts continue to indicate the existence of the open separation line on the side. For Reynolds numbers less than about  $2.5 \times 10^5$ , however, a closed

separation bubble (flow reversal) was also observed near the tail (Figure 25(a)) in addition to the separation bubble near the maximum radius location.

- (b) At higher Reynolds numbers (about  $7 \times 10^5$ ), the separation bubble near the nose does not disappear (see Figure 25(b)) but the closed separation near the tail decreases in extent and exists only on the leeward side of the tail region.

Again it is seen that for the combination body the Reynolds number as well as the angle of attack influences the overall flow pattern. Since the closed separation near the nose was absent at high Reynolds numbers and moderate angles of attack, it was concluded that the combination body was suitable for the detailed boundary layer explorations.



## CHAPTER V

## DISCUSSION

Thus far, the discussion of the flow visualization study has centered around the identification of the qualitative features of the surface streamlines on bodies of revolution at incidence and the separation patterns associated with them. The basic ideas available in the literature concerning three-dimensional separation appear to have been verified. Specifically, it has been seen that the two basic types of separation identified by Maskell (1955), and Wang (1972), are present on a body of revolution over a range of incidences. The present study has also illustrated the possible streamline configurations in somewhat greater detail than heretofore, particularly with respect to the location of the singular points of the surface streamlines and the origin of the open types of separation and reattachment.

Since, as stated earlier, a long-term objective of the present study was to identify a body shape on which detailed three-dimensional (turbulent) boundary-layer measurements could be made and compared with some of the emerging calculation procedures, it is natural to enquire whether there is any theoretical evidence which could be compared with the various observations made here in laminar flow. Although there is intensive on-going research effort in the area of

high-speed high-angle-of-attack aerodynamics in connection with missiles and aircraft, it is observed that there are, relatively, only a few successful computations of three-dimensional boundary layers on bodies of revolution at angles of attack - whether the boundary layer is laminar or turbulent. In some instances, the geometries that have been considered are quite simple (e.g., cones). The flow past a spheroid has been studied theoretically by Wang in a series of recent papers (Wang, 1970, 1971, 1972, 1974, 1975, and 1976). His computations were made at Reynolds numbers low enough for the boundary layer to be laminar everywhere. Some measurements are also available for the spheroid in the experiments of Wilson (1971).

Figure 26 shows the location of the points of flow reversal (S1 and S2) on the windward and the leeward sides of the plane of symmetry deduced from the photographs taken during the course of the present study. These are compared with the observations of Wilson (1971) who used smoke to visualize the flow and made some boundary layer measurements on the leeward side of the plane of symmetry of a 4:1 spheroid. Also shown are the results of the plane of symmetry calculations of Wang (1972) for a 4:1 spheroid. It should be mentioned that the equations of the three-dimensional boundary layer can be simplified considerably for the flow in a plane of symmetry (see, for example, Nash and Patel, 1972) and can be solved independently of the flow elsewhere on the body. Wang (1972) used an explicit finite-difference method to obtain his solutions.

It will be seen from Figure 26(a) that the variation with

incidence of the observed point of singular separation on the windward plane of symmetry is in good agreement with the predictions of Wang (1972). There is, however, a consistent and large discrepancy in the precise location which is not explained by the fact that the axis ratios of the spheroids used in the experiments and calculations are somewhat different. Some of the discrepancy could be due to the use of the potential-flow pressure distribution instead of the actual pressure distribution in the boundary layer computations of Wang (1972). Figure 26 shows that in axisymmetric flow the present observations are in good agreement with the experiments of Wilson and in moderate agreement with the computation made by Chang and Patel using two different methods.

The location of the singular point of separation on the leeward side of the plane of symmetry is shown in Figure 26 (b). From this it is observed that the present observations are at variance with those of Wilson and with the calculations of Wang (1972). In addition to the suspect accuracy of Wang's computations, however, the influence of the flow separation on the pressure distribution on the leeward side would invalidate the use of the potential-flow pressure distribution in the computations. The disagreement between the observations and the calculated results is therefore not altogether surprising. It should also be pointed out that the present results indicate a downstream movement of the singular separation with increasing incidences up to an incidence of about 10 to 15 degrees. The trend is then reversed for higher incidences indicating

an upstream movement of the separation point. The predictions of Wang do not follow this trend. It appears that this reversal in trend may be associated with the onset of the secondary open-type of separation, and the corresponding reattachment, since this phenomenon was observed to take place between  $\alpha = 10$  degrees and  $\alpha = 20$  degrees. The calculations based on the potential-flow pressure distribution cannot of course predict this.

In a set of later publications, Wang (1974, 1975) has reported the results of his calculations of the boundary layer on the complete spheroid (i.e., in the region between the upper and lower lines of symmetry). Figure 27 shows a comparison between his calculation for a 4:1 spheroid at  $\alpha = 6$  degrees and the present observations on the 4.3:1 spheroid at  $\alpha = 5$  degrees. The spheroid surface is represented in rectangular coordinates consisting of the axial distance  $X/L$  and the circumferential angle  $\theta$ . At these low incidences, there is a remarkable qualitative agreement between the two sets of results, in particular with respect to the shape of the closed separation line.

A similar comparison is made in Figure 28 for the higher incidence of 30 degrees. Now it is observed that there is good qualitative agreement between the predicted open separation line and the observed primary open separation line. The position of this line relative to the locus of minimum potential-flow pressure coefficient is different in the two cases and may be attributed to a strong interaction between the separated flow and the external inviscid flow. The calculations of Wang (1974, 1975) did not of course

predict either the secondary open separation or the closed separation line. The basic problems involved in performing such boundary-layer calculations are immense and their discussion is beyond the scope of the present investigation.

## CHAPTER VI

## CONCLUSIONS

The following conclusions can be drawn from the present investigation:

- (1) The boundary layer flow past a body of revolution at incidence is quite complex. Although the topology of the surface streamlines, or skin-friction lines, does not give a great deal of information concerning the overall flow pattern and its aerodynamic or hydrodynamic consequences, it enables the identification of two basic types of three-dimensional flow separations: a closed or bubble type of separation, and an open or free-vortex type of separation. Thus, the proposals of Maskell (1955) and Wang (1972) are verified by the present experiments.
- (2) The closed type of separation line is one which contains singular points of the limiting streamlines and the flow downstream of it is inaccessible from upstream. Closed separation occurs at all angles of attack on a spheroid at least at Reynolds numbers where the boundary layer is laminar.
- (3) An open type of separation line does not contain any singular points. The flow on either side of such a

separation line is accessible from upstream. Such separation occurs at high incidences on a spheroid and leads to the shedding of longitudinal vortices and the formation of a large vortical wake.

- (4) Although the precise locations of the lines of separation depend on the body shape and Reynolds number (i.e., whether the boundary layer is laminar or turbulent), the basic features of the flow in the neighborhood of such separations, when they occur, appear to be independent of Reynolds number.
- (5) The present study seems to indicate that at a given incidence the lines of open separation terminate at nodal points of separation on the line of closed separation.
- (6) Limited tests indicate that the combination body is suitable for further experimental work. The line of transition to turbulent flow is expected to be earlier than on other shapes, and therefore sufficiently thick turbulent boundary layers will be available for detailed boundary-layer measurements. At sufficiently high Reynolds numbers, the closed separation bubble on the tail of this body is expected to be small or nonexistent.
- (7) Some comparisons have been made between the results of the flow-visualization experiments and the few available theoretical calculations. These appear

to be in qualitative agreement. Possible reasons for the quantitative discrepancies have been discussed.

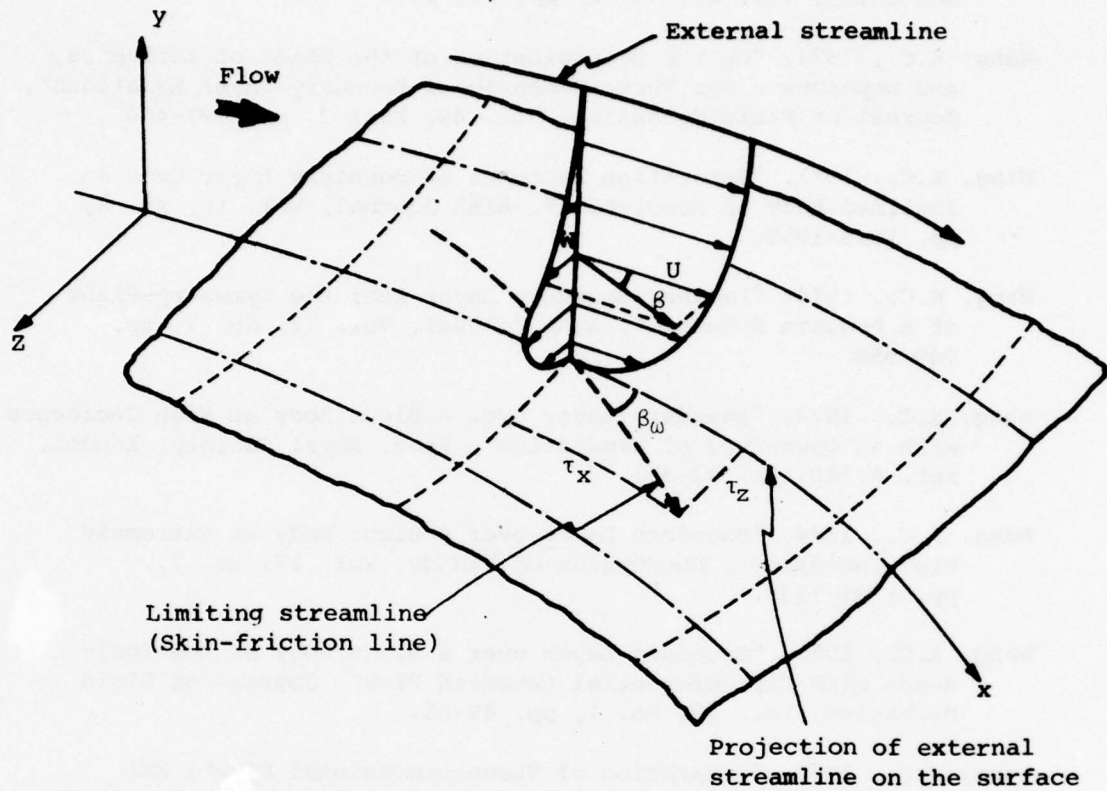
- (8) This study has helped to identify the basic features of three-dimensional boundary-layer separations on a body of revolution at incidence. This would assist in making meaningful measurements and computations in the detailed study that is planned.



## REFERENCES

- Brown, S.N. and Stewartson, K., 1969, "Laminar Separation", Annual Review of Fluid Mechanics, Vol. 1.
- Chang, K.C. and Patel, V.C., 1975, "Calculation of Three-Dimensional Boundary Layers on Ship Forms", IIHR Report No. 178, Iowa Institute of Hydraulic Research, The University of Iowa, Iowa City, Iowa.
- Choi, D.H., 1977, Private Communication.
- Eichelbrenner, E.A. and Oudart, A., 1954, "Observations on a Criterion of Three-Dimensional Laminar Boundary-Layer Separation", Rech. Aéron., No. 40, pp. 3-5. Also: NRC (Canada) TT-962, 1961.
- Eichelbrenner, E.A., 1973, "Three-Dimensional Boundary Layers", Annual Review of Fluid Mechanics, Vol. 5.
- Goodson, R.E. and Parsons, J.S., 1972, "The Optimum Shaping of Axisymmetric Bodies for Minimum Drag in Incompressible Flow", Automatic Control Center, School of Mech. Eng., Purdue University, Rept. ACC-72-5.
- Lighthill, M.J., 1963, "Laminar Boundary Layers", Edited by L. Rosenhead, Oxford University Press, Oxford, England.
- Maskell, E.C., 1955, "Flow Separation in Three-Dimensions", RAE Report Aero 2565, Royal Aircraft Establishment, Bedford, England.
- Moore, F.K., 1956, "Three-Dimensional Boundary Layer Theory", Advances in Applied Mechanics, Vol. 4, Academic Press, New York.
- Nash, J.F. and Patel, V.C., 1972, "Three-Dimensional Turbulent Boundary Layers", SBC Technical Books.
- Patel, V.C., Lee, Y.-T., and Güven, O., 1977, "Measurements in the Thick Axisymmetric Turbulent Boundary Layer and the Near Wake of a Low-Drag Body of Revolution", Presented at the Turbulent Shear Flows Symposium, Pennsylvania State University, April 18-20, 1977. To be published in the Proceedings.
- Peake, D.J., Rainbird, W.J., and Atraghji, E.G., 1972, "Three-Dimensional Flow Separations on Aircraft and Missiles", AIAA Journal, Vol. 10, No. 5, pp. 567-580

- Smith, J.H.B., 1975, "A Review of Separation in Steady Three-Dimensional Flow", AGARD-CP-No. 168, Paper III-31.
- Wang, K.C., 1970, "Three-Dimensional Boundary Layer Near the Plane of Symmetry of a Spheroid at Incidence", Journal of Fluid Mechanics, Vol. 43, No. 1, pp. 187-209.
- Wang, K.C., 1971, "On the Determination of the Zones of Influence and Dependence for Three-Dimensional Boundary-Layer Equations", Journal of Fluid Mechanics, Vol. 48, Part 2, pp. 397-404.
- Wang, K.C., 1972, "Separation Patterns of Boundary Layer Over an Inclined Body of Revolution", AIAA Journal, Vol. 10, No. 8, pp. 1044-1050.
- Wang, K.C., 1974, "Laminar Boundary Layer Near the Symmetry-Plane of a Prolate Spheroid", AIAA Journal, Vol. 12, No. 7, pp. 949-958.
- Wang, K.C., 1974, "Boundary Layer over a Blunt Body at High Incidence with an Open-Type of Separation", Proc. Royal Society, London, Ser. A.340, pp. 33-35.
- Wang, K.C., 1974, "Boundary Layer over a Blunt Body at Extremely High Incidence", The Physics of Fluids, Vol. 17, No. 7, pp. 1381-1385.
- Wang, K.C., 1975, "Boundary Layer over a Blunt Body at Low Incidence with Circumferential Reversed Flow", Journal of Fluid Mechanics, Vol. 72, No. 1, pp. 49-65.
- Wang, K.C., 1976, "Separation of Three-Dimensional Flow", MML TR-76-54C, Martin Marietta Laboratories, Baltimore, Maryland.
- Wilson, G.R., 1971, "Experimental Study of a Laminar Boundary Layer on a Body of Revolution", Master's thesis, GAM/AE/71-4, Air Force Institute of Technology, Wright-Patterson Air Force Base, Ohio.



$U$  = Velocity component along the external streamline.

$W$  = Velocity component normal to the external streamline.

$\beta$  = Cross-flow angle.

$\beta_\omega$  = Wall cross-flow angle.

Figure 1. Three-Dimensional Boundary Layer: Definition Sketch

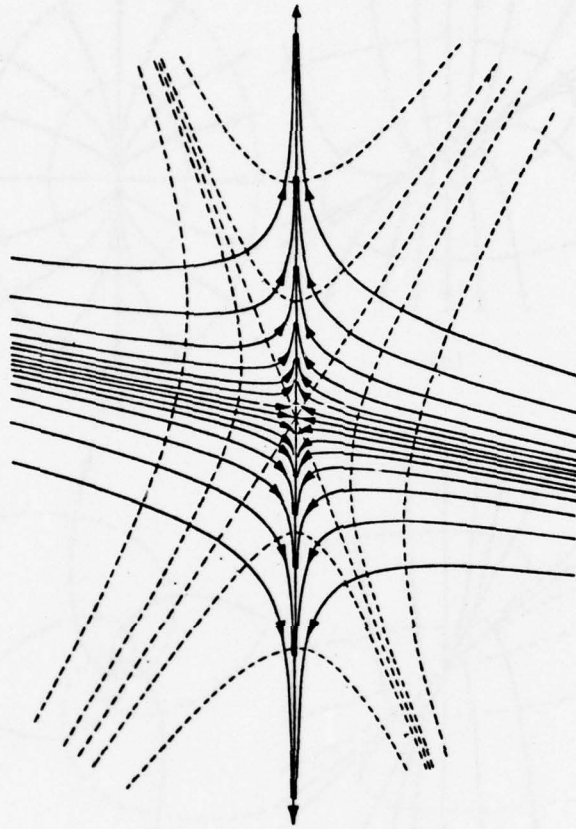


Figure 2. Typical Pattern of Skin-Friction Lines (full) and Vortex Lines (broken) near a Saddle Point of Separation

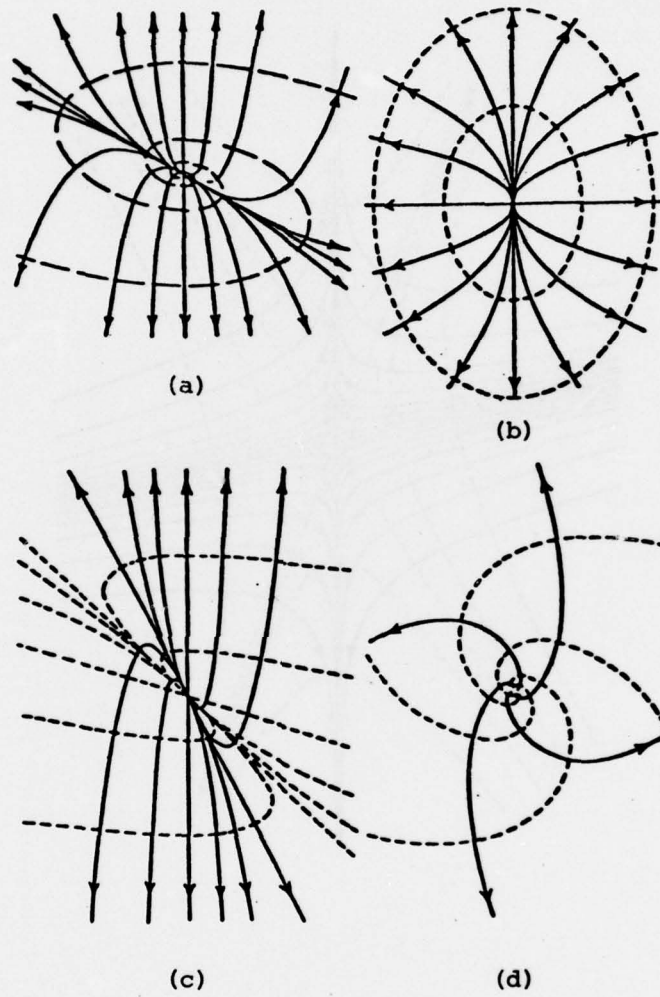


Figure 3. Limiting Streamlines and Vortex Lines near Nodal Points of Attachment

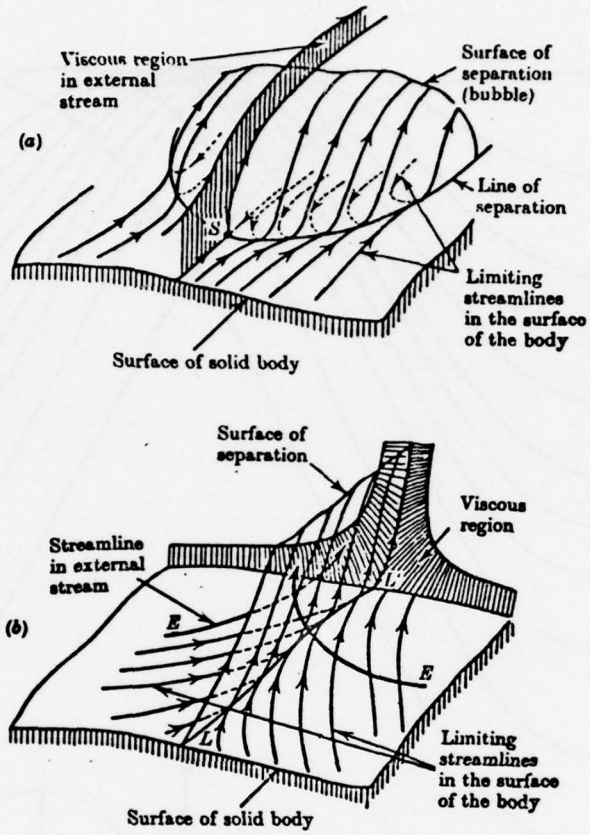
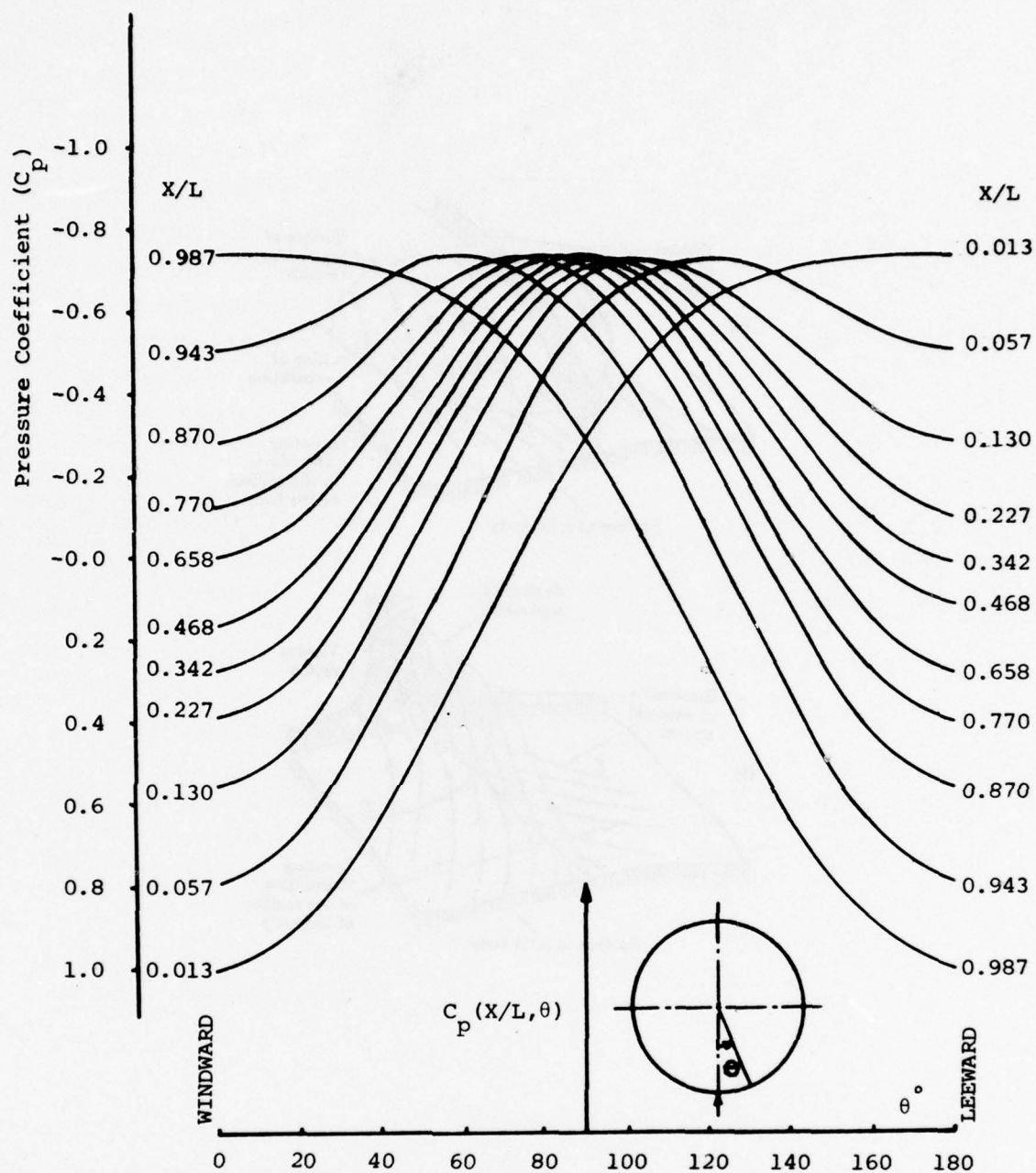
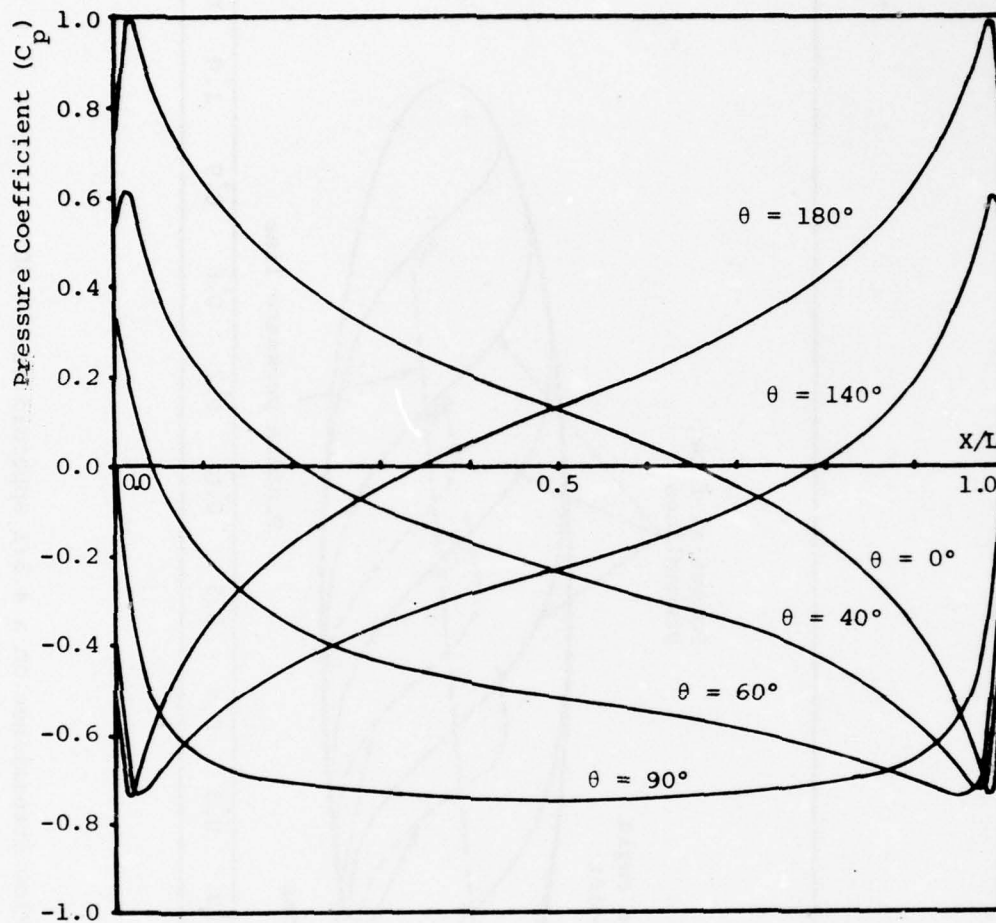


Figure 4. Two Models of Three-Dimensional Separations  
(Maskell, 1955)



(a) Circumferential Direction

Figure 5. Potential-Flow Pressure Distributions over a 4.3:1 Spheroid at  $30^\circ$  Incidence



(b) Longitudinal Direction

Figure 5. (cont'd)



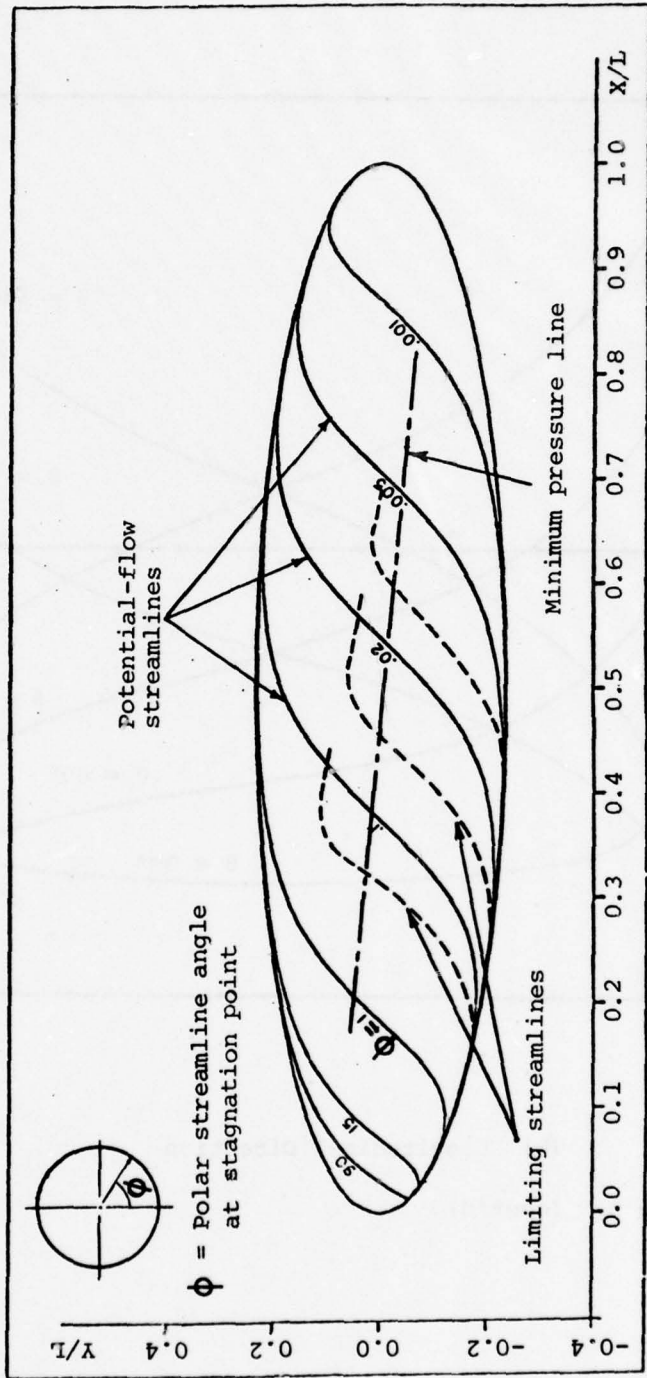


Figure 6. Potential-Flow Streamlines on a 4.3:1 Spheroid at  $\alpha = 30^\circ$

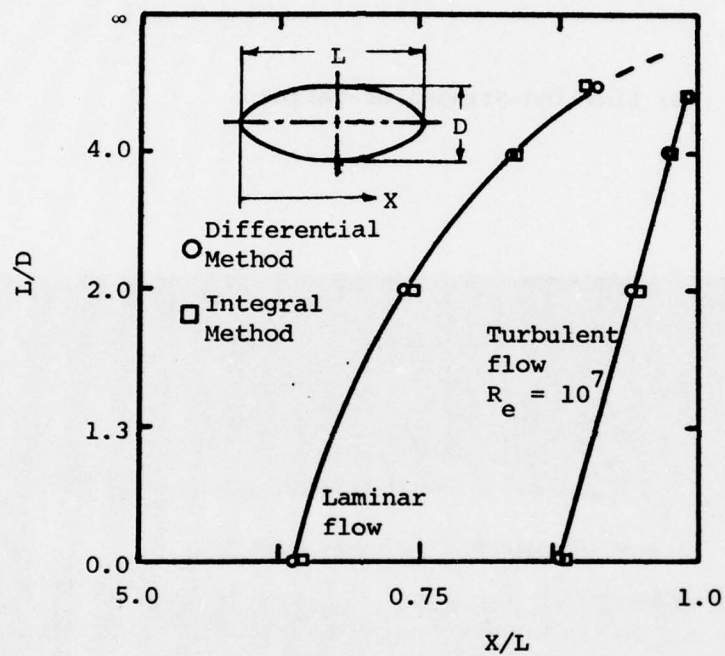
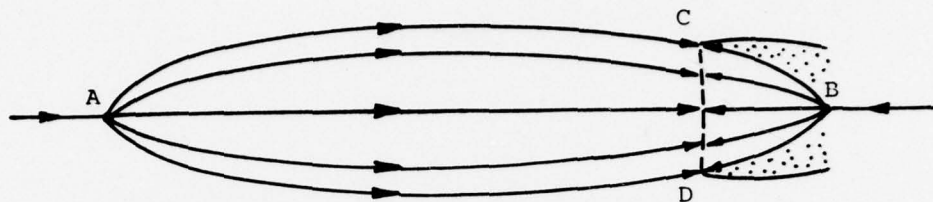
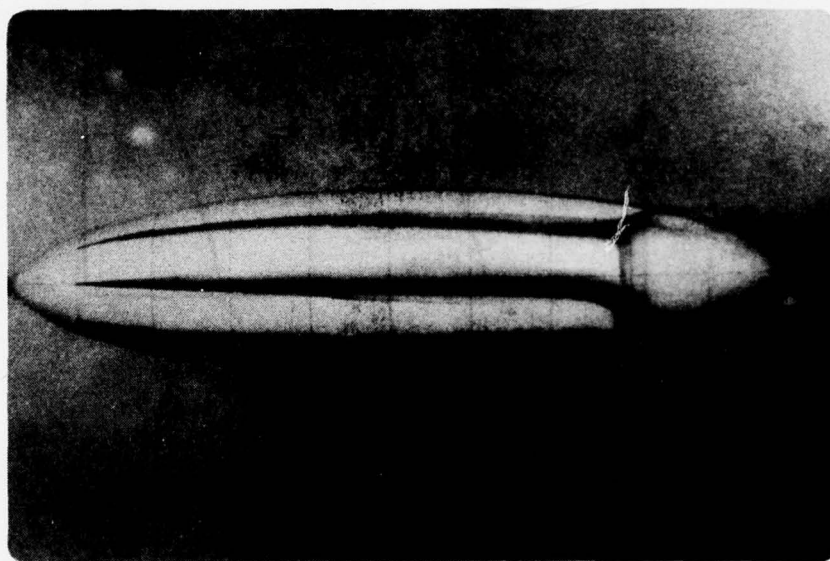


Figure 8. Locations of Axisymmetric Separation on Spheroid (Chang and Patel, 1975)

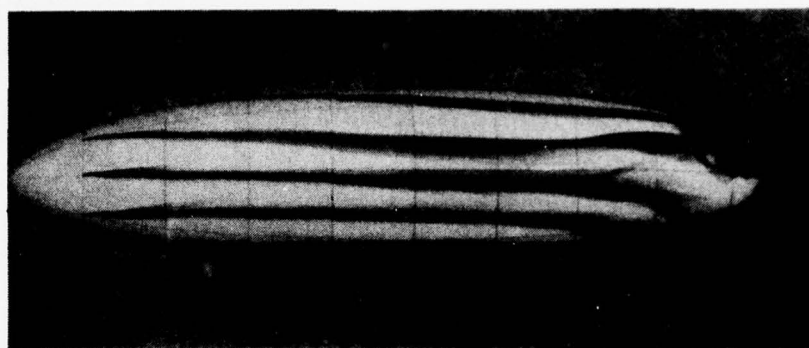


(a) Limiting Streamline Pattern

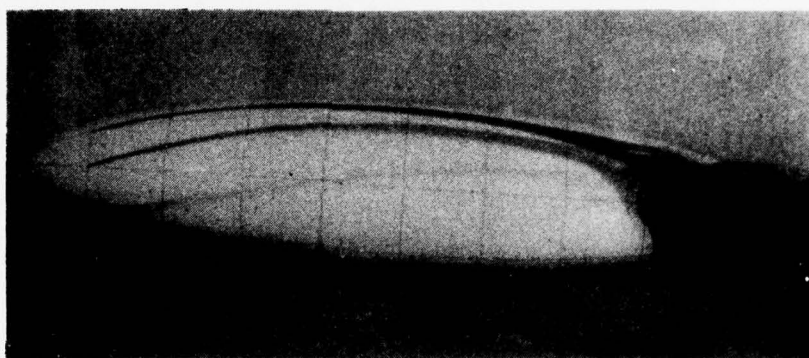


(b) Dye Streak-line Pattern

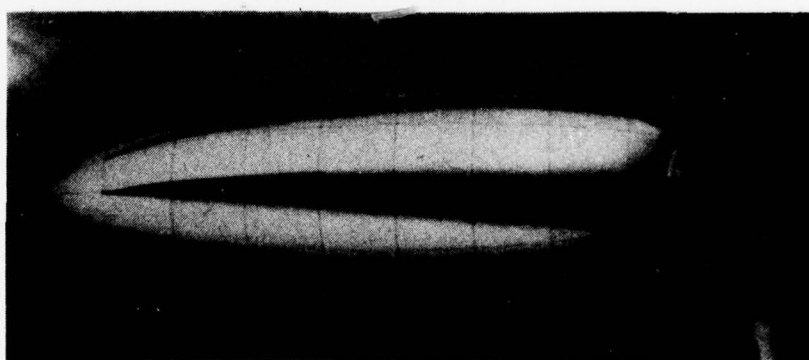
Figure 7. Flow Past a Spheroid at Zero Incidence



(a) Top View (Leeward)

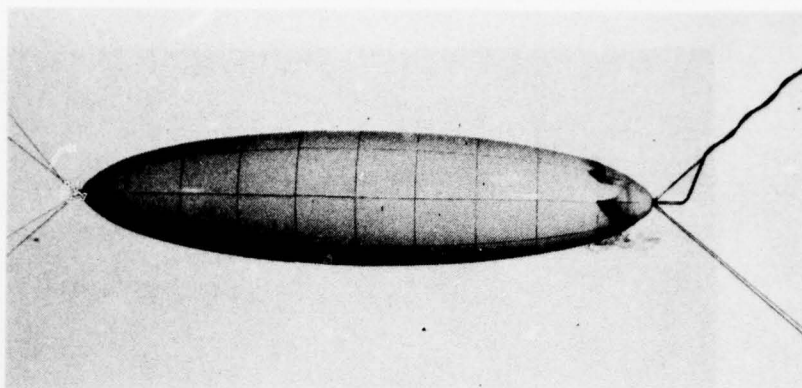


(b) Side View

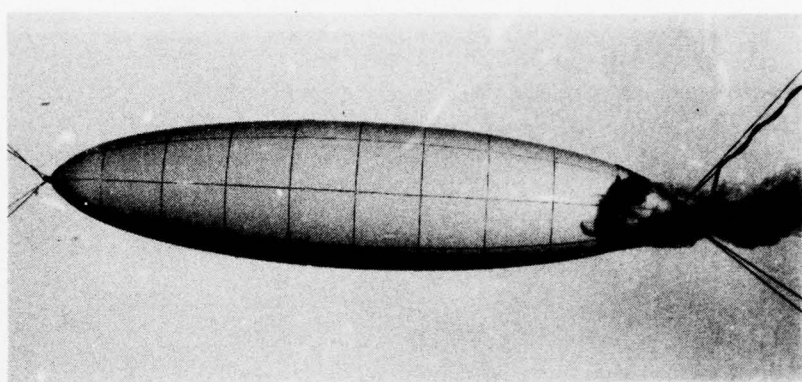


(c) Bottom View (windward)

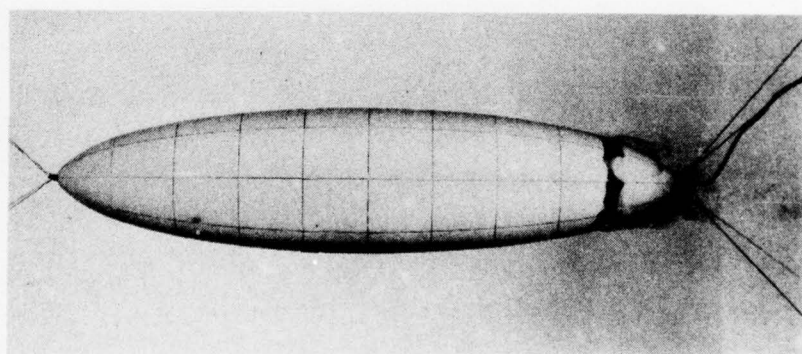
Figure 9. Flow Past a Spheroid at  $5^\circ$  Incidence



(a) Top View

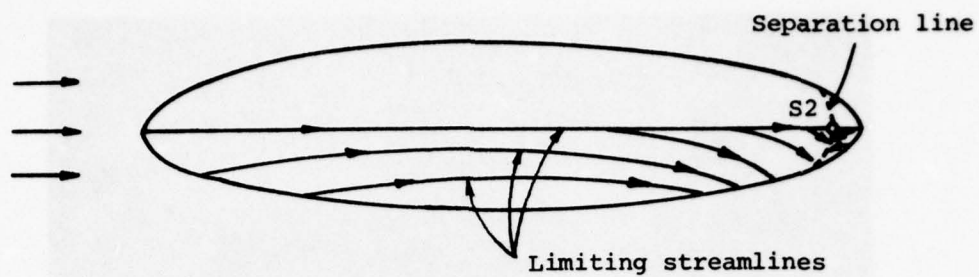


(b) Side View

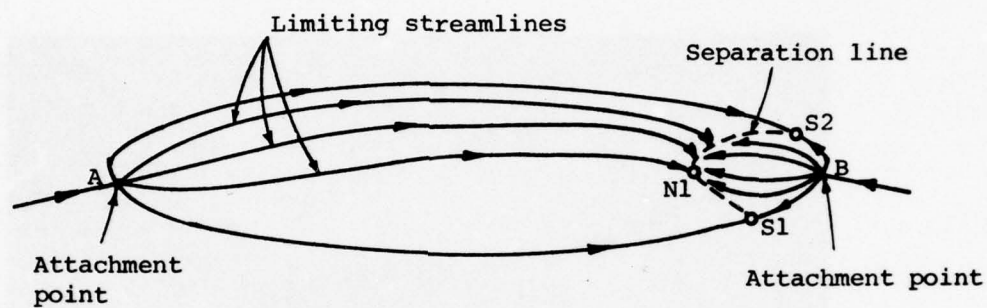


(c) Bottom View

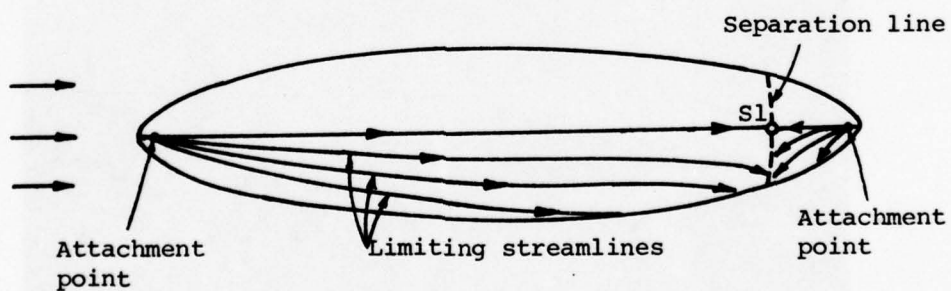
Figure 10. Flow Past a Spheroid at  $5^\circ$  Incidence



(a) Top View

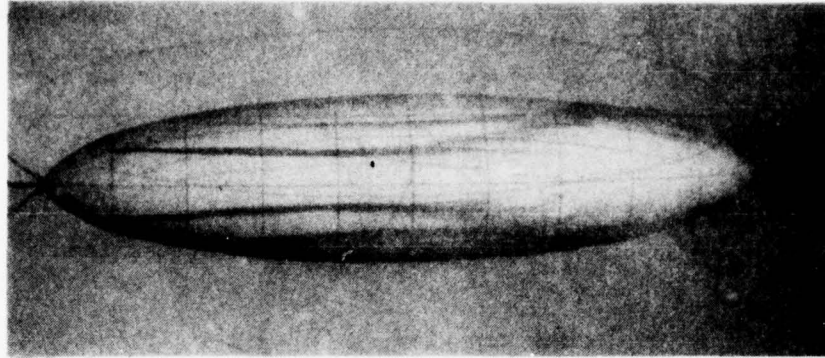


(b) Side View

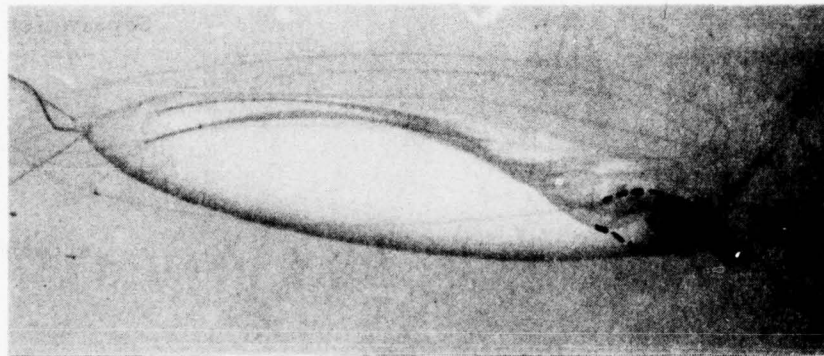


(c) Bottom View

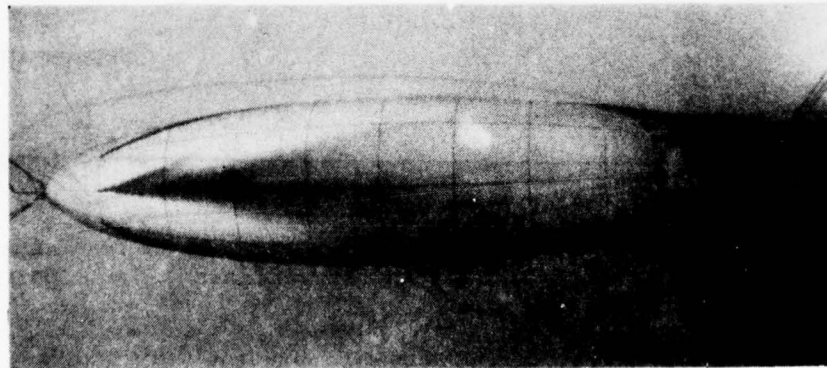
Figure 11. Surface Flow Patterns at Low Incidence ( $\alpha = 5^\circ$ )



(a) Top View

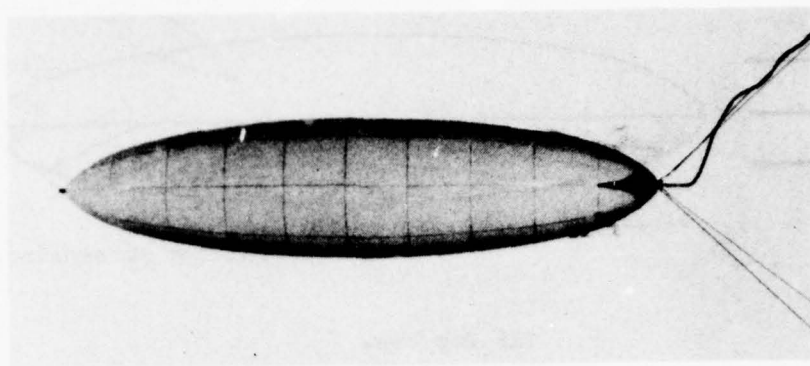


(b) Side View

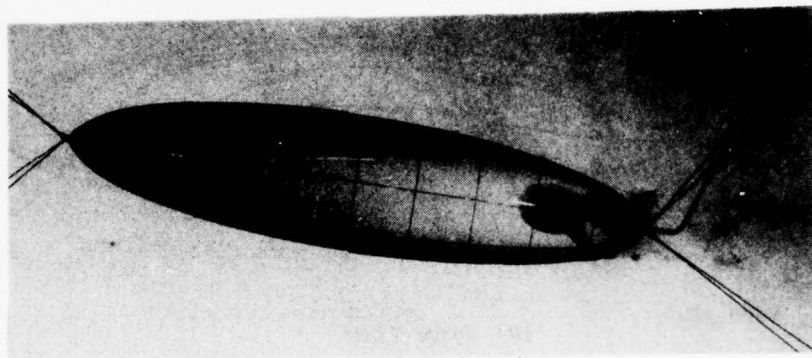


(c) Bottom View

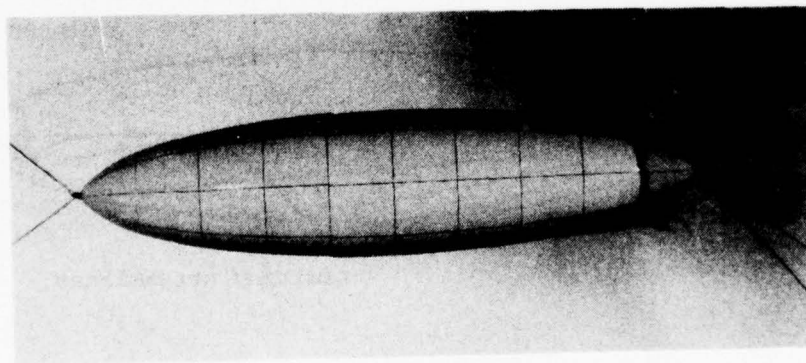
Figure 12. Flow Past a Spheroid at  $10^\circ$  Incidence



(a) Top View



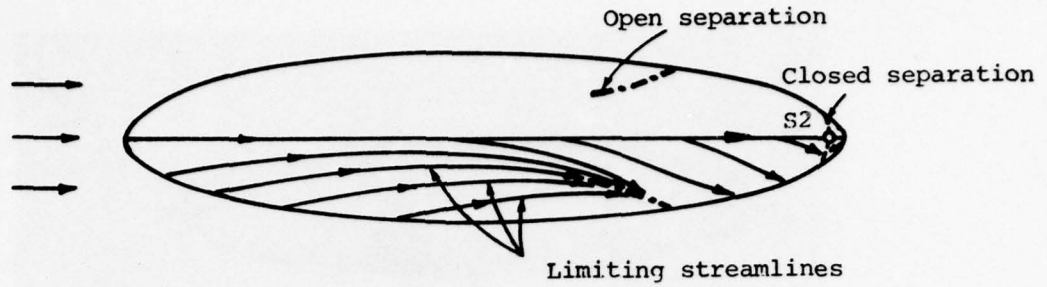
(b) Side View



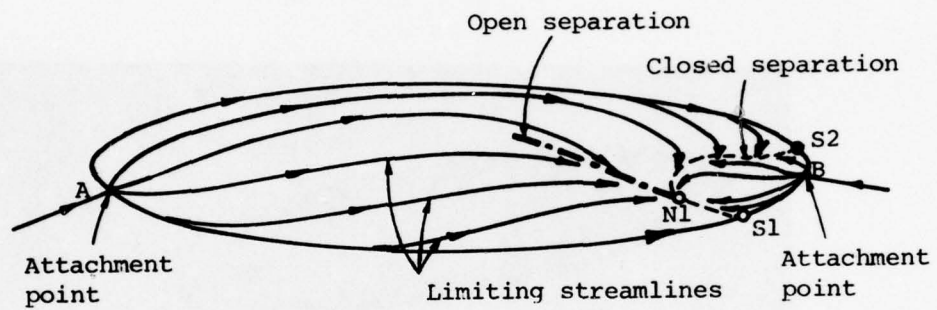
(c) Bottom View

Figure 13. Flow Past a Spheroid at  $10^\circ$  Incidence

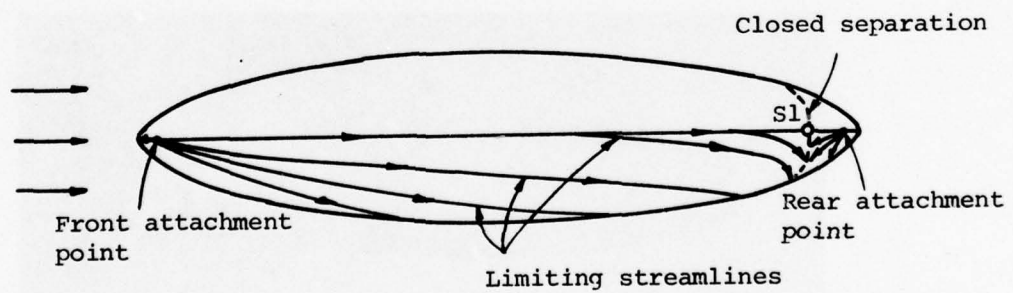




(a) Top View

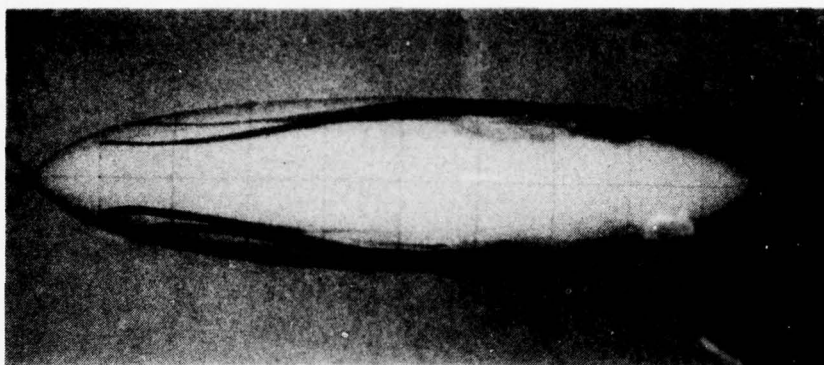


(b) Side View

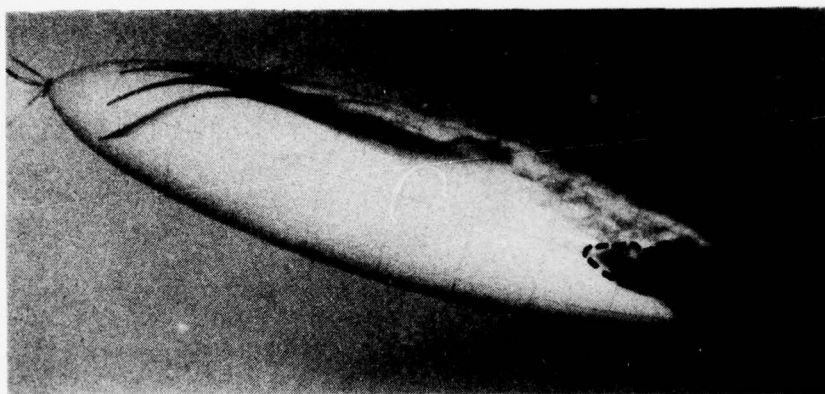


(c) Bottom View

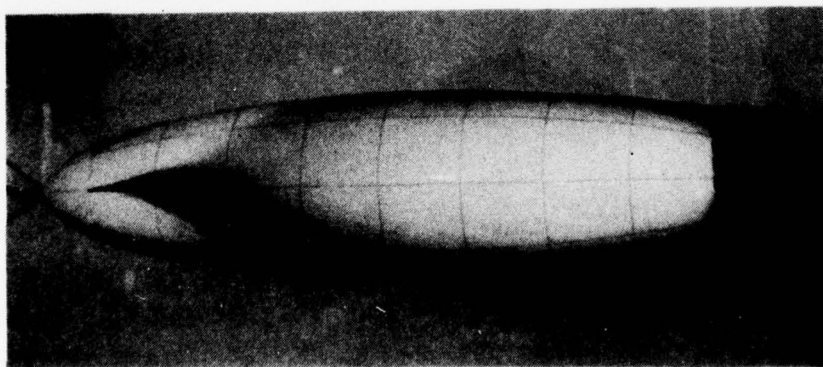
Figure 14. Surface Flow Patterns at Moderate Incidence ( $\alpha = 10^\circ$ )



(a) Top View

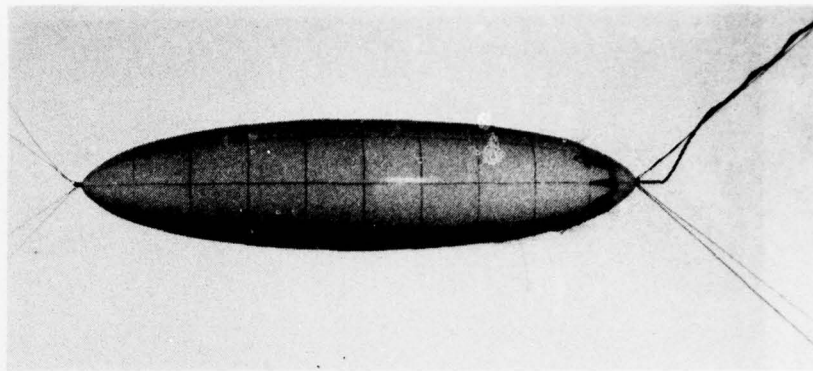


(b) Side View

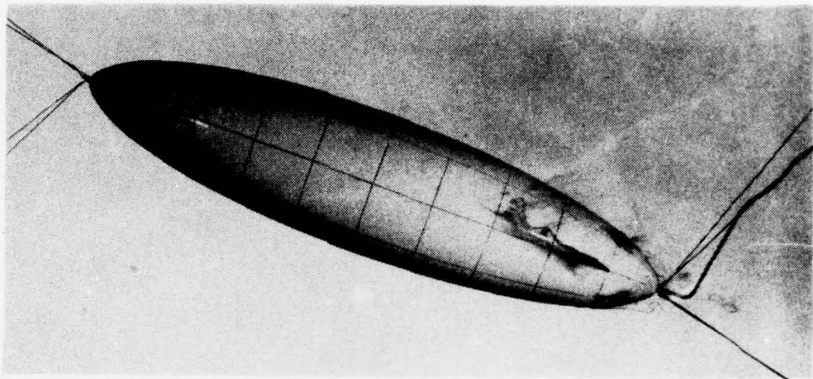


(c) Bottom View

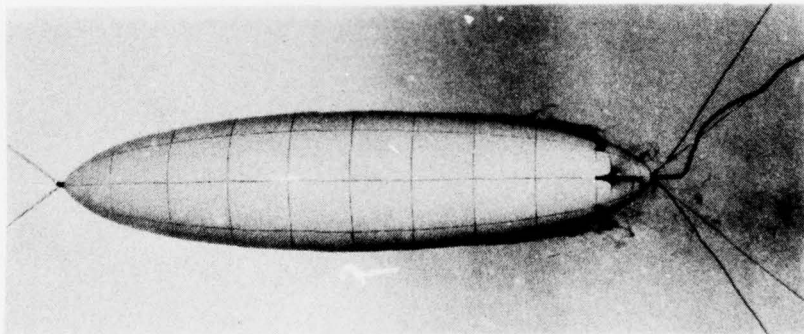
Figure 15. Flow Past a Spheroid at  $20^\circ$  Incidence



(a) Top View

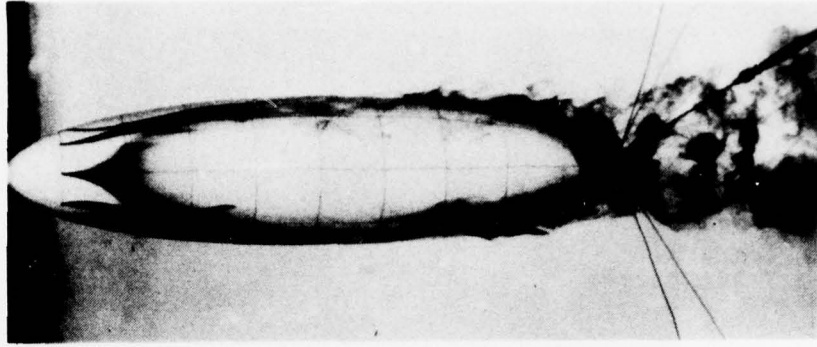


(b) Side View

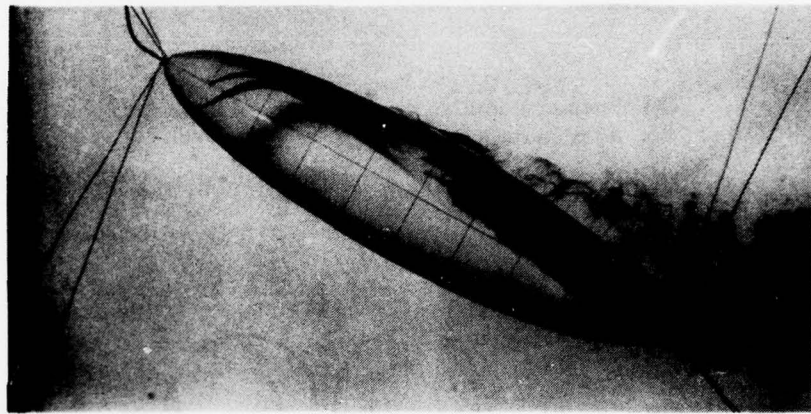


(c) Bottom View

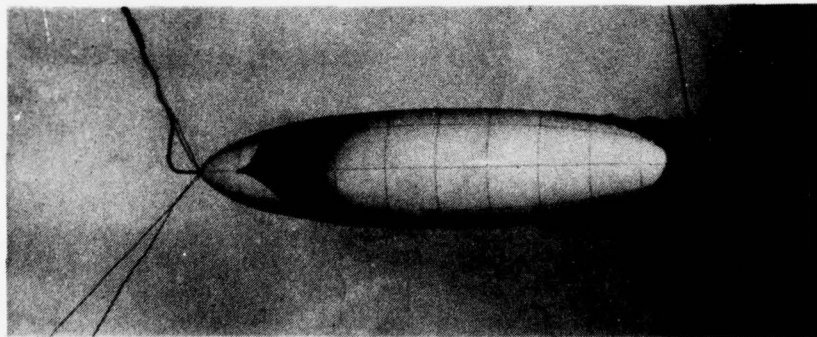
Figure 16. Flow Past a Spheroid at  $20^\circ$  Incidence



(a) Top View

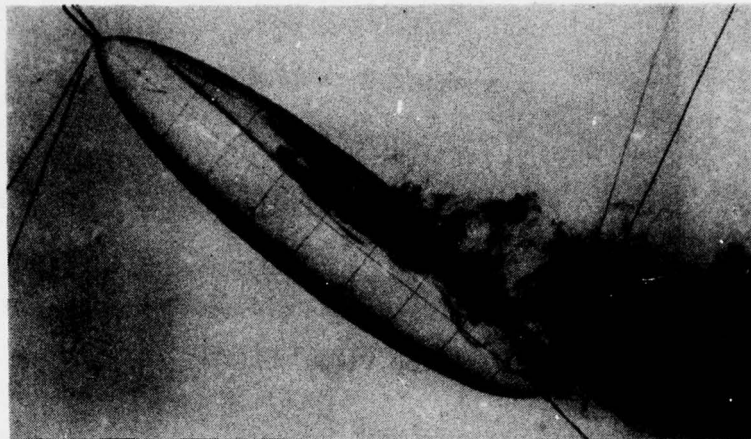


(b) Side View

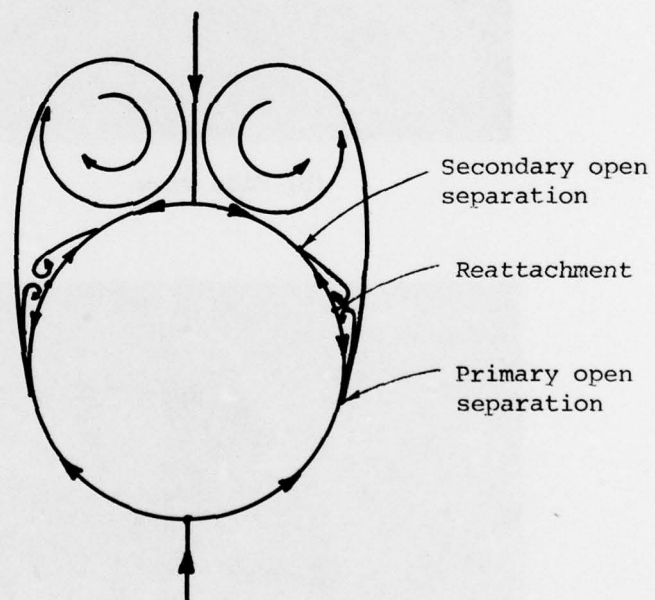


(c) Bottom View

Figure 17. Flow Past a Spheroid at  $30^\circ$  Incidence

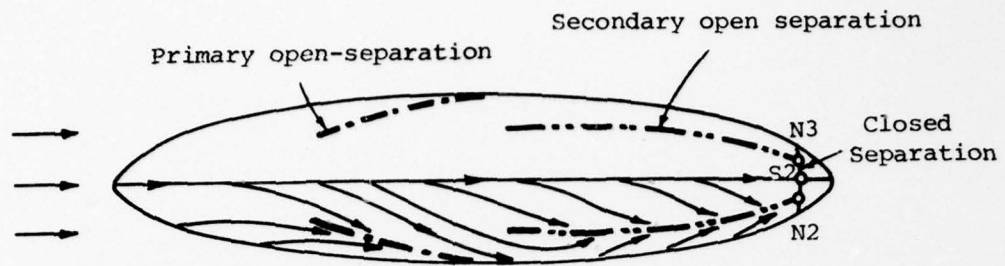


(a) Primary and Secondary Open Separations and Reattachment ( $\alpha \sim 40^\circ$ )

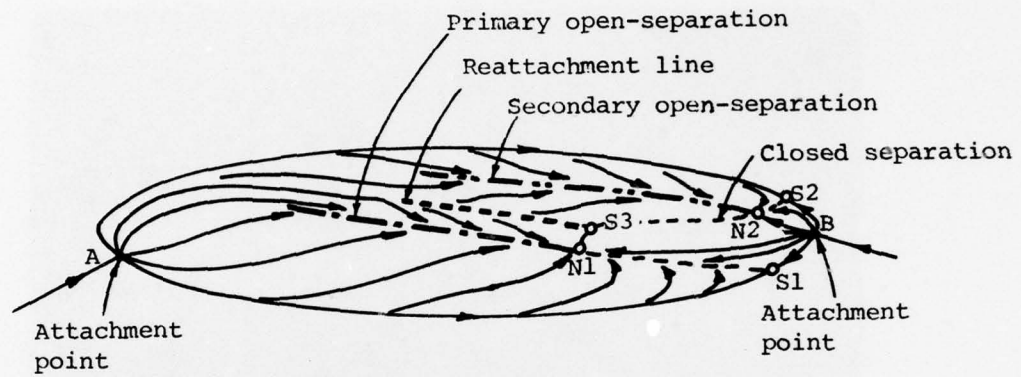


(b) Cross-Sectional View of Above

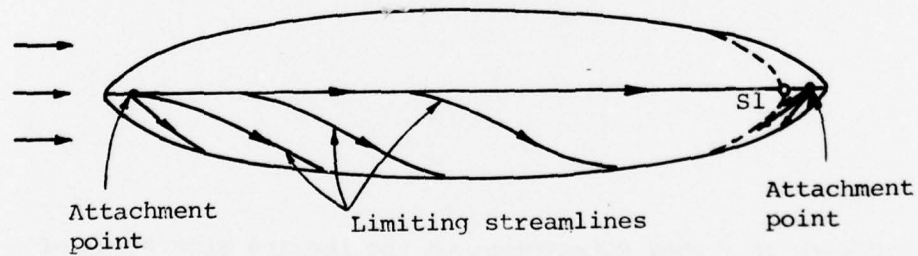
Figure 18. Illustrations of Primary and Secondary Separations



(a) Top View



(b) Side View



(c) Bottom View

Figure 19. Surface Flow Patterns at High Incidence ( $\alpha = 30^\circ$ )

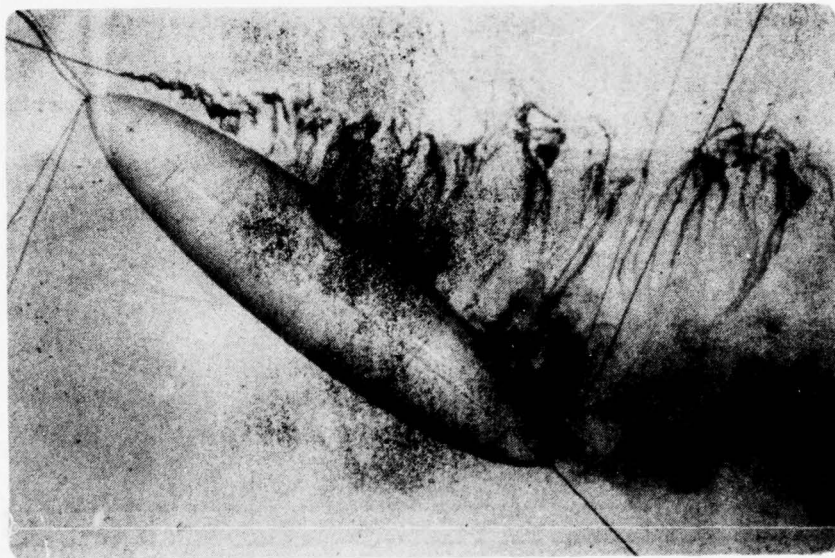
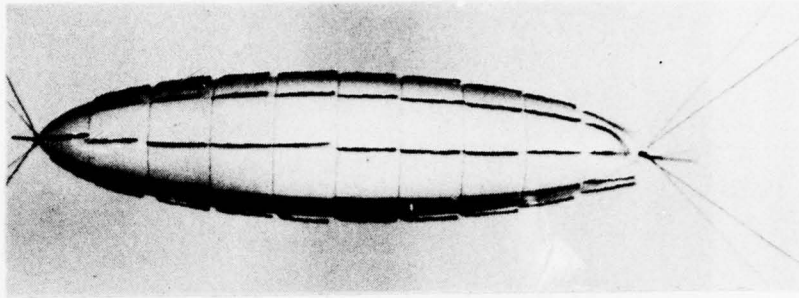
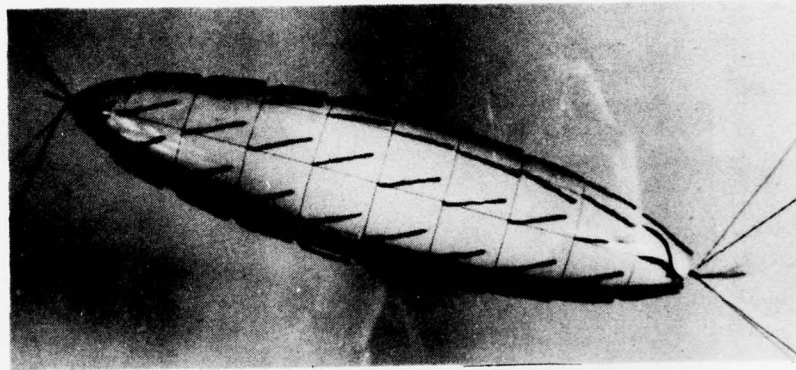


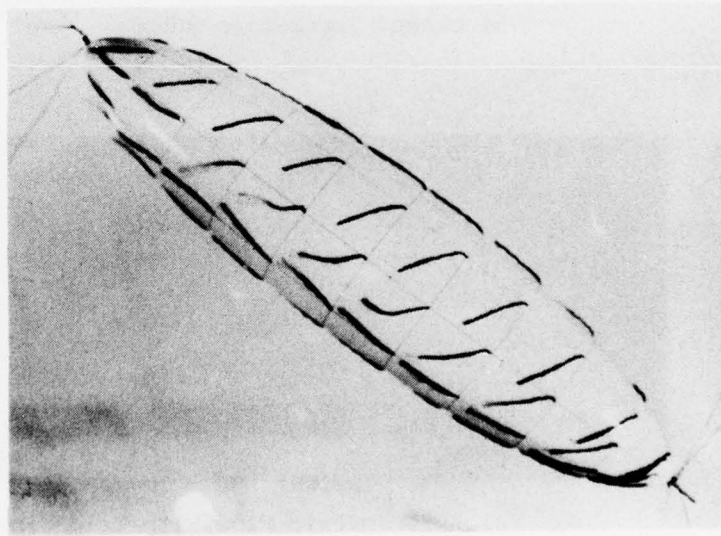
Figure 20. Flow Entrainment on the Leeward Side Plane of Symmetry ( $\alpha \sim 40^\circ$ )



(a) Axisymmetric Flow



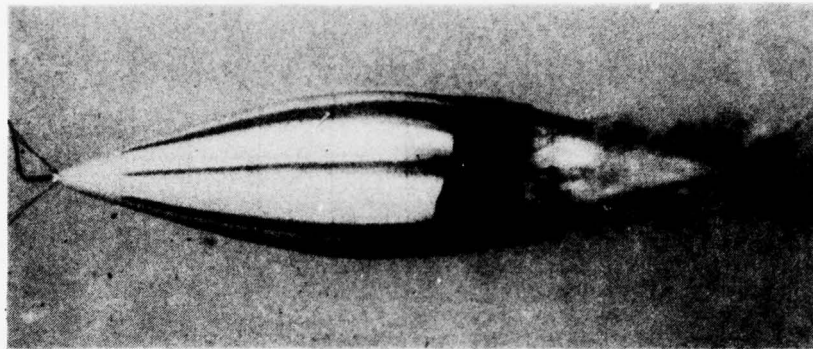
(b) Incidence of 20 degrees



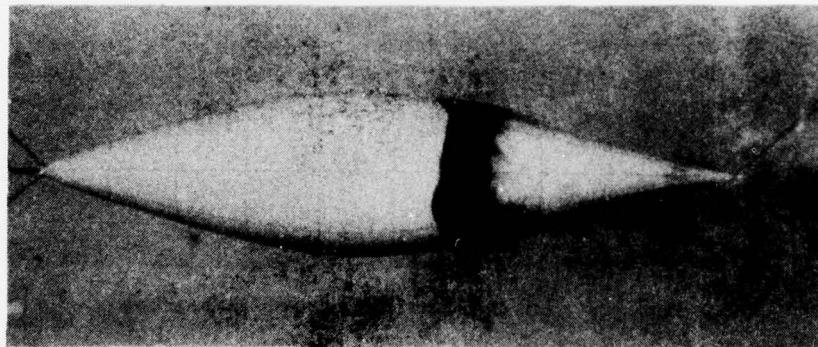
(c) Incidence of 40 degrees

Figure 21. Flow Past a Spheroid at  $R_e = 7 \times 10^5$

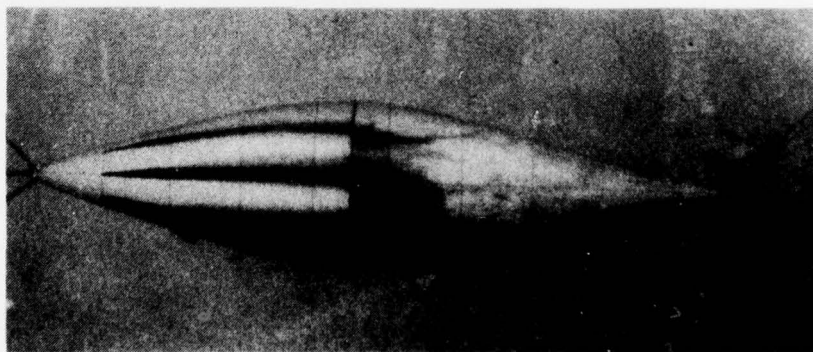




(a) Axisymmetric Flow without Trip Wire

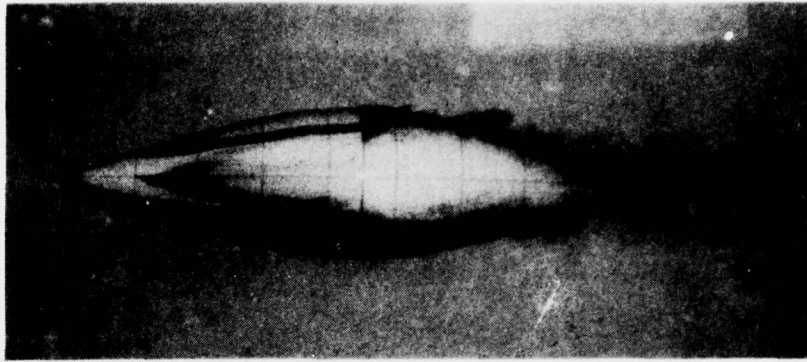


(b) Closed Separation Bubble

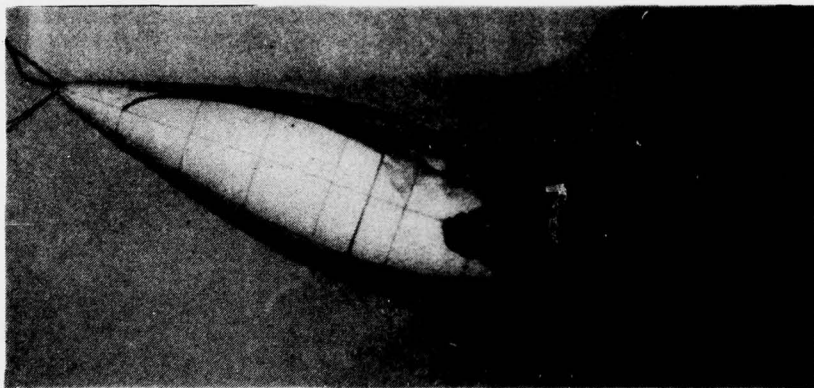


(c) Axisymmetric Flow with Trip Wire

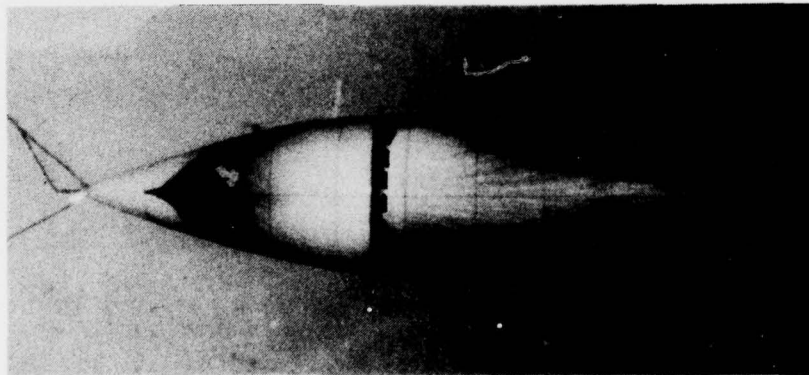
Figure 22. Flow Past a Low-Drag Body at Zero Incidence



(a) Top View

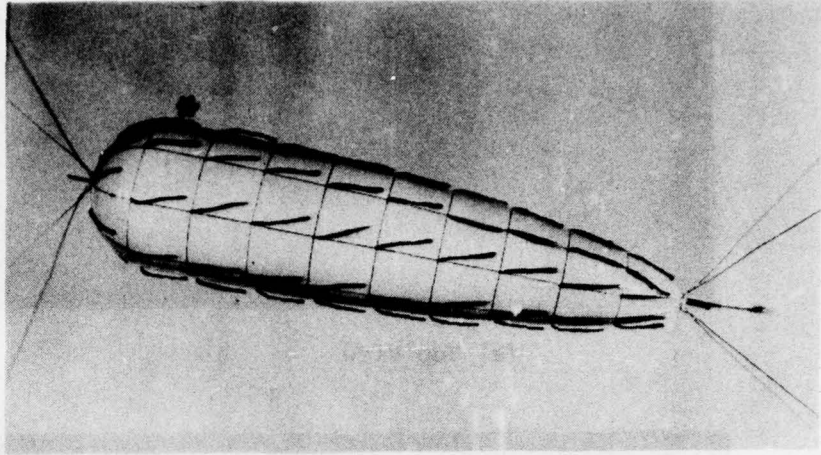


(b) Side View

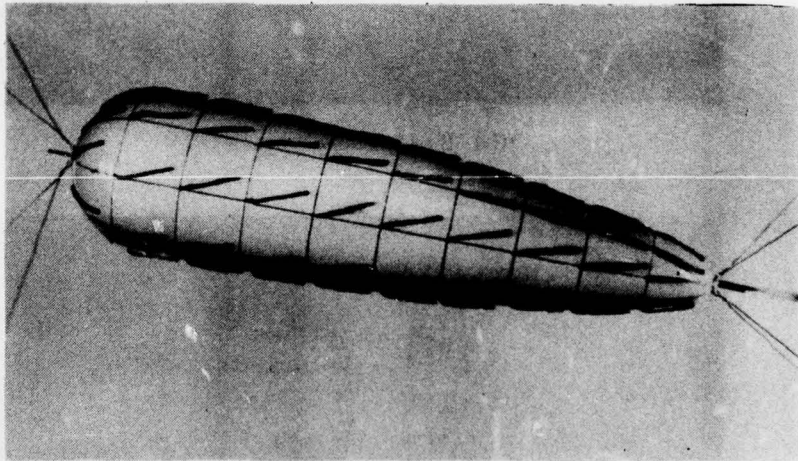


(c) Bottom View

Figure 23. Flow Past a Low-Drag Body at  $20^\circ$  Incidence

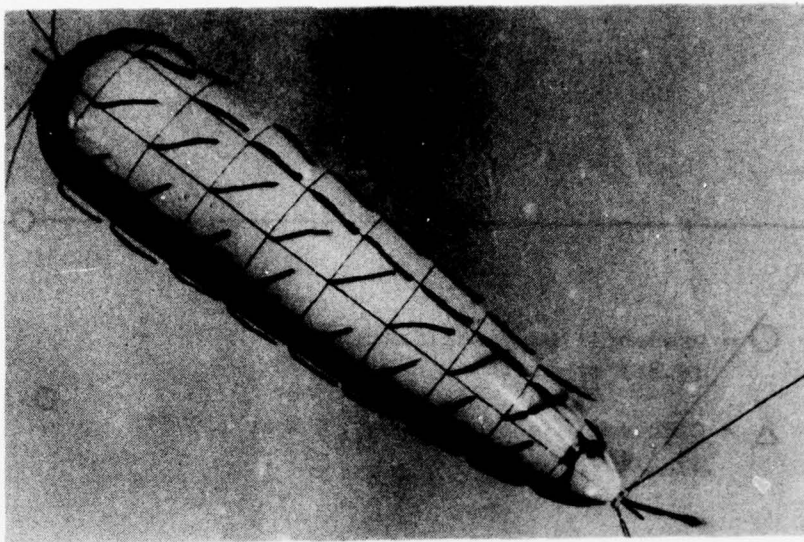


(a) Flow Pattern at  $R_e = 2.4 \times 10^5$   
(\* Note Reversed Flow Here)

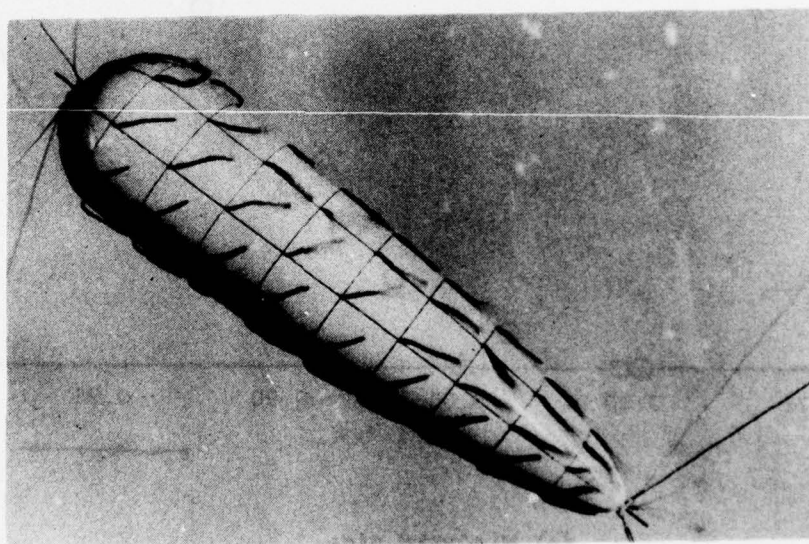


(b) Flow Pattern at  $R_e = 7.0 \times 10^5$

Figure 24. Flow Past a Combination Body at  $10^\circ$  Incidence

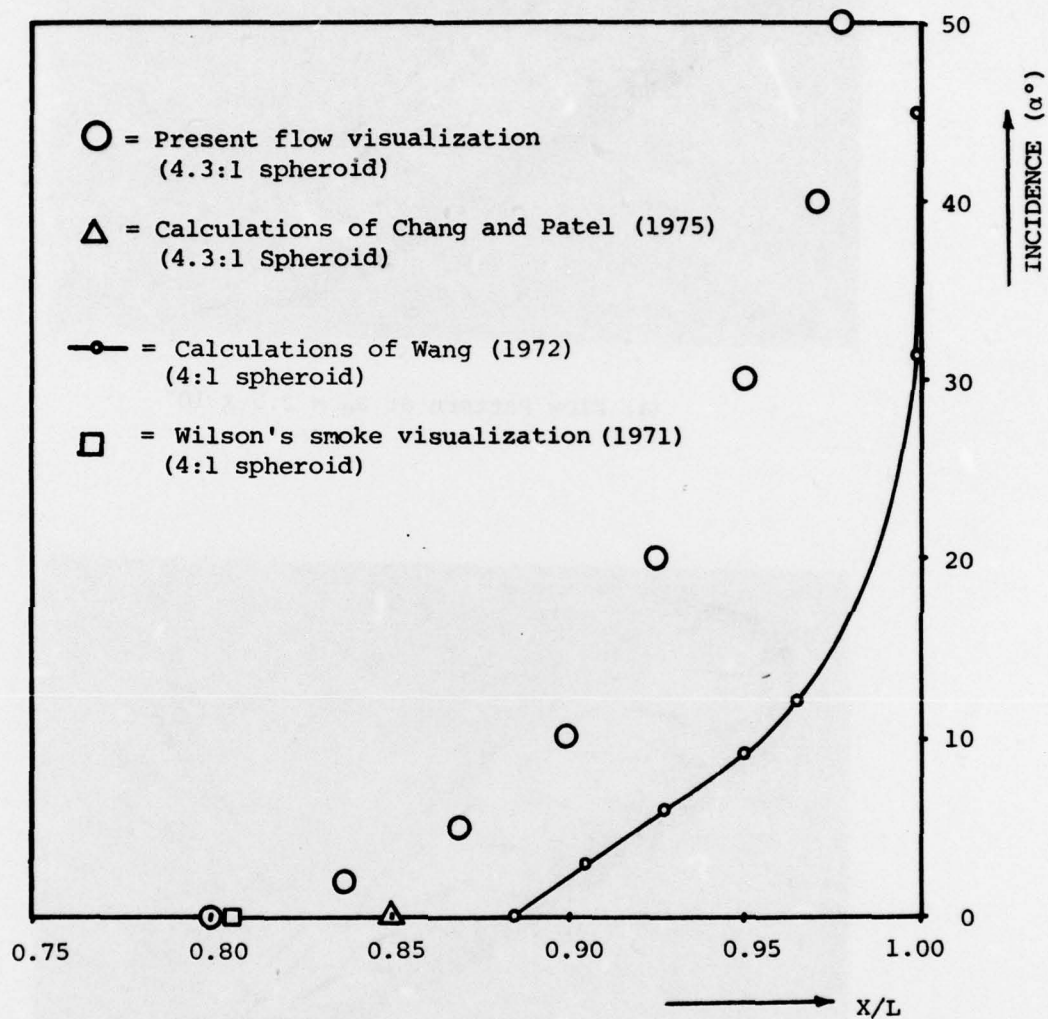


(a) Flow Pattern at  $Re = 2.5 \times 10^5$



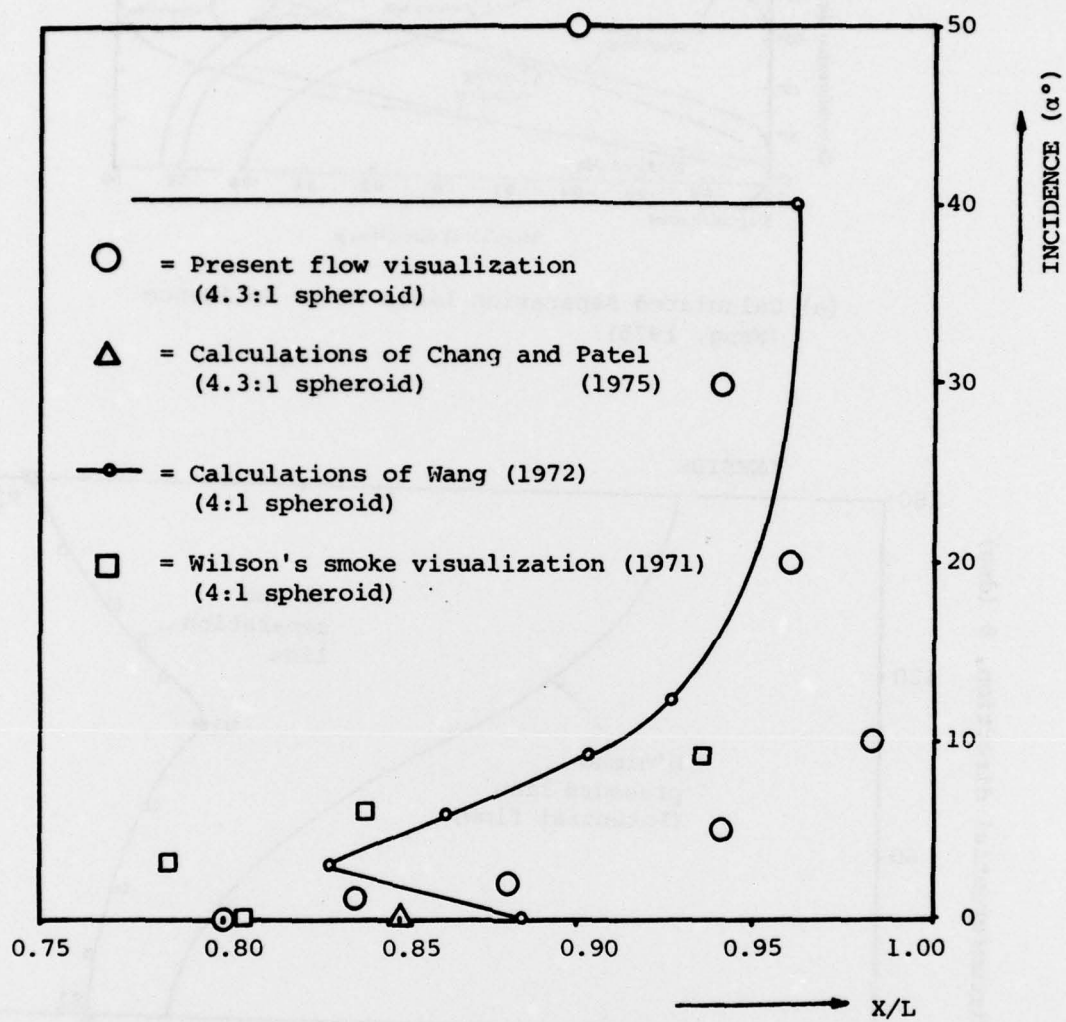
(b) Flow Pattern at  $Re = 7.0 \times 10^5$

Figure 25. Flow Past a Combination Body at  $40^\circ$  Incidence



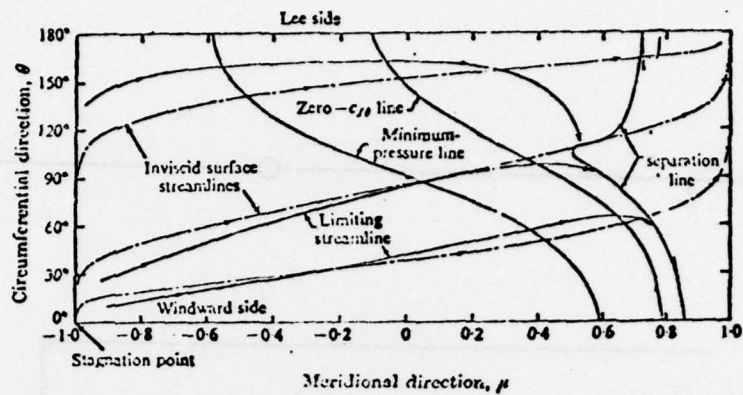
(a) Windward Side

Figure 26. Locations of Separation Point on the Plane of Symmetry of a Spheroid

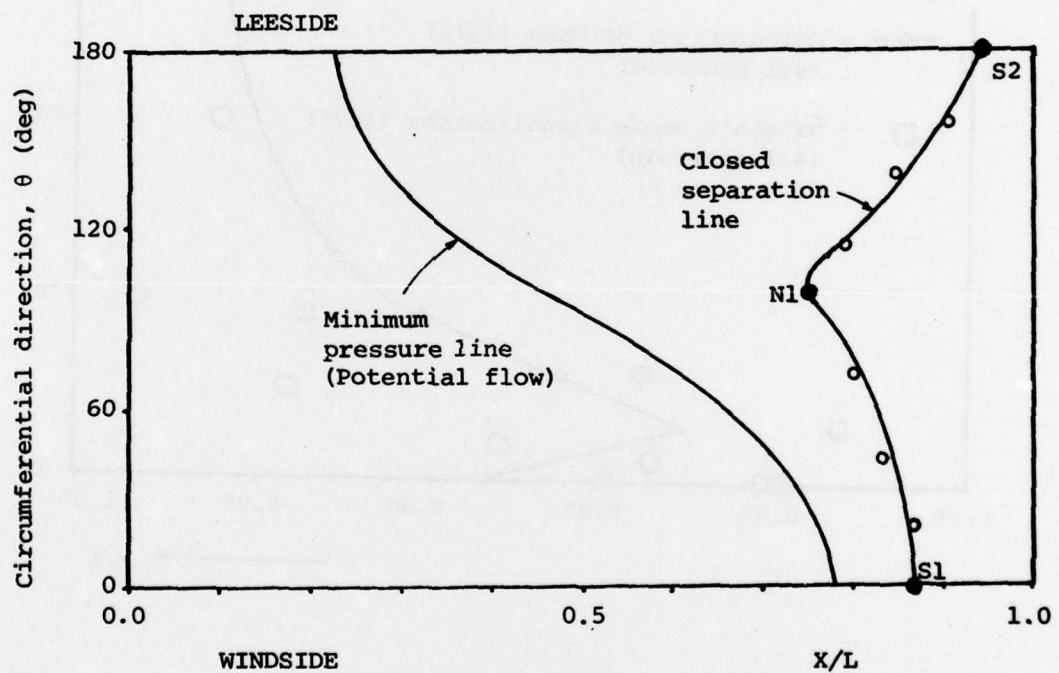


(b) Leeward Side

Figure 26. (cont'd)

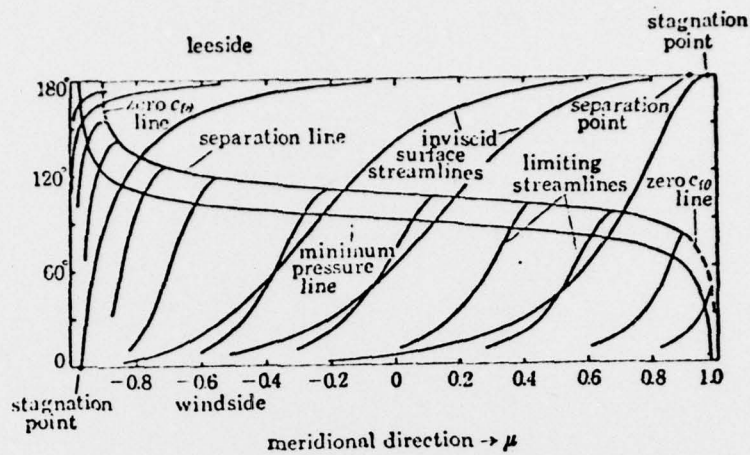


(a) Calculated Separation Lines at 6° Incidence  
(Wang, 1975)

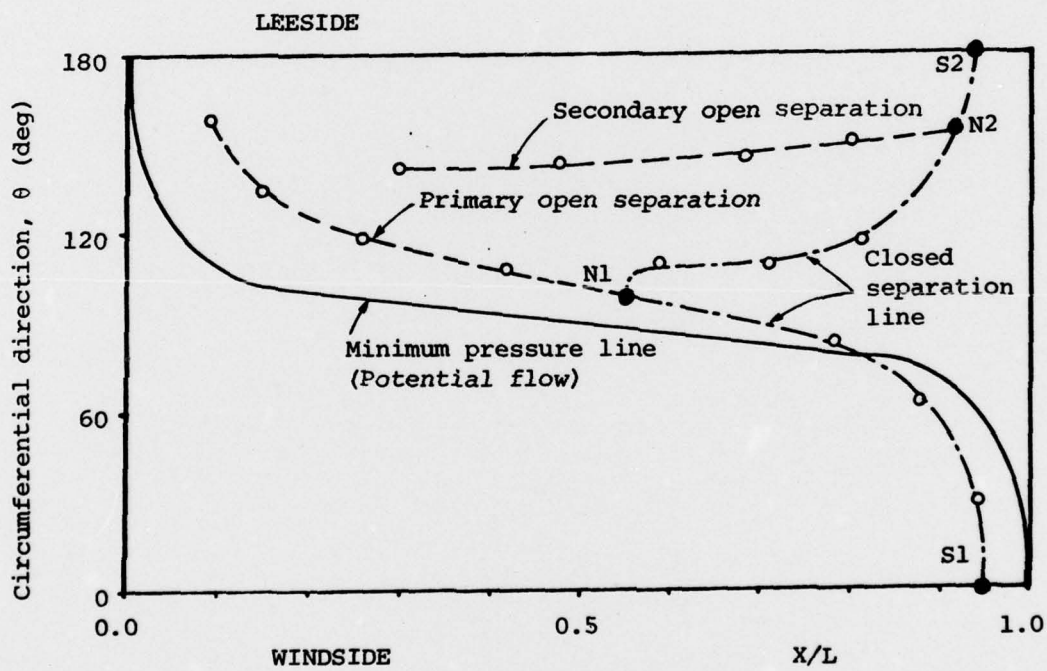


(b) Separation Lines from the Flow Visualization at 5° Incidence

Figure 27. Comparison between Calculations and Experiments at Low Incidence



(a) Calculated Separation Lines at 30° Incidence (Wang, 1974)



(b) Separation Lines from the Flow Visualization at 30° Incidence

Figure 28. Comparison between Calculations and Experiments at High Incidence